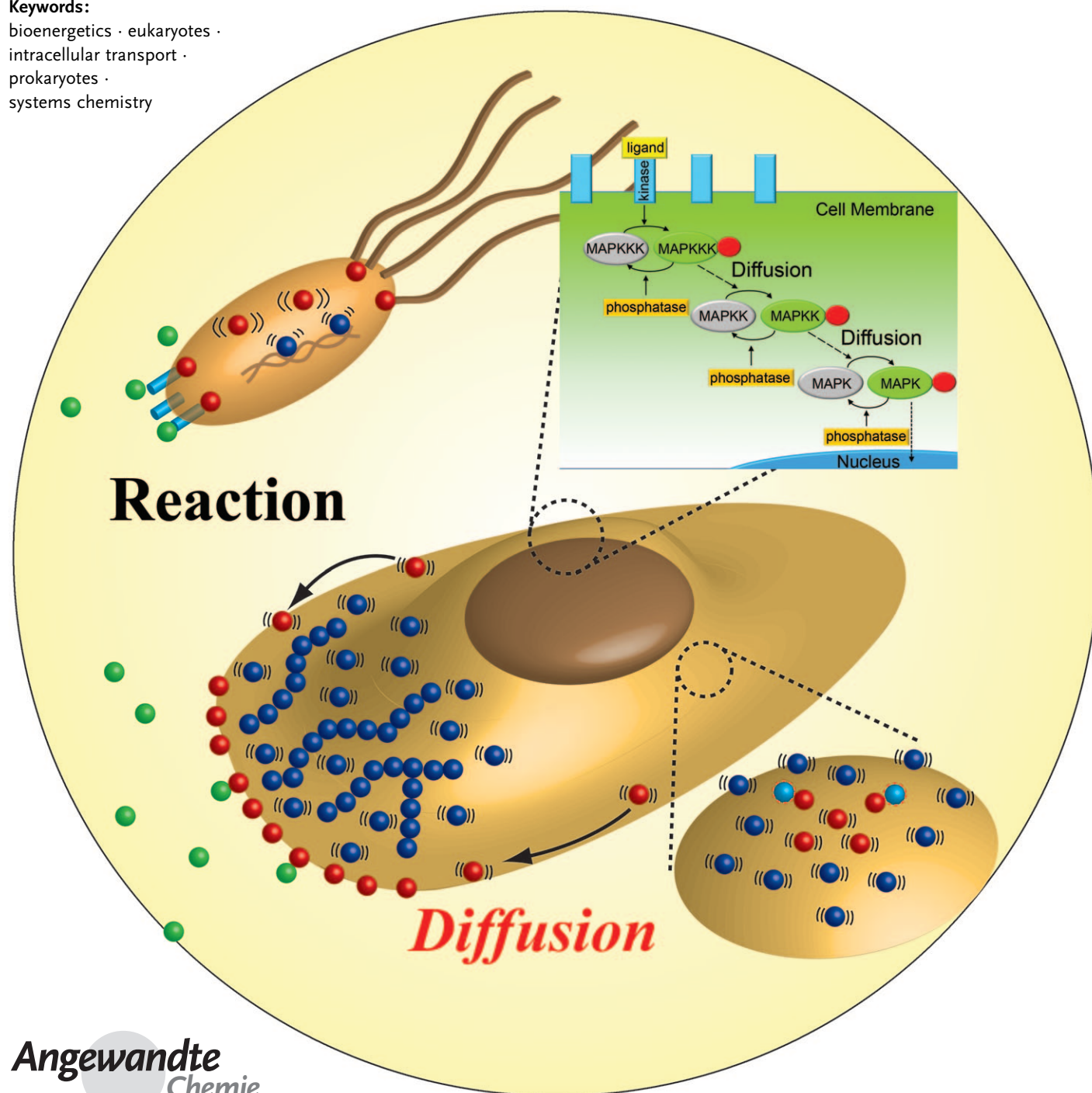# Reaction-Diffusion Systems in Intracellular Molecular Transport and Control

Siowling Soh, Marta Byrska, Kristiana Kandere-Grzybowska, and Bartosz A. Grzybowski*

Keywords:
bioenergetics · eukaryotes ·
intracellular transport ·
prokaryotes ·
systems chemistry

*C*hemical reactions make cells work only if the participating chemicals are delivered to desired locations in a timely and precise fashion. Most research to date has focused on active-transport mechanisms, although passive diffusion is often equally rapid and energetically less costly. Capitalizing on these advantages, cells have developed sophisticated reaction-diffusion (RD) systems that control a wide range of cellular functions—from chemotaxis and cell division, through signaling cascades and oscillations, to cell motility. These apparently diverse systems share many common features and are "wired" according to "generic" motifs such as nonlinear kinetics, autocatalysis, and feedback loops. Understanding the operation of these complex (bio)chemical systems requires the analysis of pertinent transport-kinetic equations or, at least on a qualitative level, of the characteristic times of the constituent subprocesses. Therefore, in reviewing the manifestations of cellular RD, we also describe basic theory of reaction-diffusion phenomena.

From the Contents

1. Introduction

A cell is much more than a sac of uniformly distributed molecules that react with one another. Instead, the function-

Table 1: Examples of active, nondiffusive intracellular transport.

Transport modality	Manifestations and function
Long-range, motor-based transport along microtubules	1. vesicular transport 1.1. movement of endosomes/endocytic compartments (phagocytosis, pinocytosis, and receptor-mediated endocytosis)[75,278,279] uptake and movement of macromolecules (internalization of cell-surface receptors), other cells (phagocytosis), fluids, and solutes (pinocytosis) enclosed in vesicles from the external environment into the cell. 1.2. exocytosis[75] transport of vesicles containing newly synthesized proteins and lipids from the endoplasmic reticulum to the trans-Golgi network and their secretion to the cell exterior. 2. bidirectional transport (that is, from the cell interior to the periphery and vice versa) of membrane-enclosed organelles (e.g. mitochondria)[280,281] and macromolecules (e.g. proteins,[81] mRNAs[282]) by kinesin and dynein motors.[283]
Short-range, motor-based transport along actin filaments	transport of membrane organelles,[284–286] mRNAs,[282] and proteins.[287]
Carrier-mediated active transport through membranes	ATP-dependent transport of: 1. ions (e.g. Na$^+$-K$^+$ pump-mediated transport of sodium ions out of a cell coupled with the transport of potassium ions into the cell; most important in nerve and muscle cells to generate electrical signals).[75,288] 2. specific molecules against the concentration gradient (e.g., transport of iodine by thyroid gland cells).[75,288]

ing of cells is crucially dependent on the proper synchronization of biochemical reactions with the timely and precise delivery of the participating chemicals.[1] Recent advances in in-cell imaging by using fluorescent protein (green fluorescent protein (GFP) and other spectral derivatives) fusions[2–7] and the development of sensors for detecting molecular interactions and conformational changes[8] have enabled unprecedented possibilities for tracking individual (bio)molecules, for quantitative determination of intracellular concentration profiles of interacting proteins, and for studying various modes of intracellular transport. The majority of this research has concentrated on the more-elaborate "active" transport mechanisms (Table 1) and has, to some extent, overlooked the simplest mode of cellular trafficking—by diffusion—and its importance in controlling intracellular processes. This Review takes a critical look at whether and when diffusion plays an important role in controlling biochemical reactions inside cells. Above all, we wish to analyze how the coupling between diffusion and reaction can give rise to complex, intracellular reaction-diffusion (RD) systems capable of feedback, amplification, oscillation, intracellular pattern formation, formation of supramolecular structures, or taxis.

This Review is aimed at chemists and biochemists—rather than biologists or biophysicists—for three reasons. First, the subject matter of diffusive transport and chemical kinetics has historically been part of a chemical curriculum.[9–11] Although some mathematical aspects of coupled reaction-diffusion phenomena might not be so familiar, the underlying concepts

[*] S. Soh, M. Byrska, Prof. K. Kandere-Grzybowska
Department of Chemical and Biological Engineering
Northwestern University
2145 Sheridan Rd, Evanston, IL 60208 (USA)

Prof. B. A. Grzybowski
Department of Chemistry, Department of Chemical and Biological Engineering, Northwestern University
2145 Sheridan Rd, Evanston, IL 60208 (USA)
E-mail: grzybor@northwestern.edu
Homepage: http://www.dysa.northwestern.edu

of concentration gradients, fluxes, or reaction orders are well known to chemists, and extending them to describe RD processes should be relatively straightforward. Second, and probably most important, it is often chemists who nowadays invent new tools with which to image in-cell transport and reactions. Indeed, the 2008 Nobel Prize[5–7] for the discovery of GFP and related proteins is a spectacular achievement by two chemists (and, of course, a biologist, M. Chalfie). In addition, it is also chemists who work vigorously on the development of new spectroscopic methods (for example, stochastic optical reconstruction microscopy[12,13] (STORM), stimulated emission depletion[14,15] (STED), photoactivated localization microscopy[16] (PALM), nonlinear structured-illumination microscopy[17]) and nanoprobes (gold nano-rods,[18–20] "nanocages",[21,22] iron oxide nanoparticles,[23–25] and semiconductor quantum dots[26–28]) for intracellular imaging. The study of RD in cells is one prominent area where these tools can come in handy. Third, and looking forward, cellular RD systems involving multiple reactions orchestrated in space and time by diffusion can provide inspiration for the development of "artificial" chemical systems. In this context, the emerging field of systems chemistry[29–33] can benefit from mimicking the biological ways of "hooking" reactions together into network modules that perform complex functions such as signal transduction, amplification, or even self-replication.

Throughout the Review, we will compare and contrast RD in prokaryotic and eukaryotic cells. Since prokaryotes are

simple organisms and are typically small (ca. 1 μm in diameter[34]), one might expect that even with slow diffusion they would be able to deliver molecules to desired reaction sites in relatively short times. In contrast, the use of diffusion as a molecular transport mechanism in larger eukaryotes (typically ca. ≈10–30 μm in diameter[34]) should be less important, and these cells should probably operate their reaction networks by using active intracellular transport. As we will show, these intuitive predictions are generally, but not fully, correct. Prokaryotes, indeed, predominantly use diffusive trafficking, which they couple skillfully to biochemical reactions to control processes such as chemotactic cell movement, selection of the cell center as the division site, and targeting of specific sites on DNA by proteins (Figure 1 a–c). In the eukaryotes (Figure 1 d,e), reaction-diffusion (RD) processes are not as prevalent, but they—alone or in combination with other mechanisms—are still used to control a surprisingly large portion of cellular "machinery": signaling cascades, organization of mitotic spindle, frequency entrainment through chemical waves, and the key cytoskeletal components involved in cell motility. Analysis of these and other examples prompts some intriguing questions: Why have passive transport and RD been retained in eukaryotes despite their apparent inefficiency? In which situations is it "profitable" for cells to rely on diffusive processes?

To try to answer these questions, we first have to develop some intuition about RD processes. Accordingly, we begin by discussing the basics of RD, formulate equations that describe

Siowling Soh graduated in chemical engineering from the National University of Singapore in 2002. He is currently undertaking PhD research with Prof. Bartosz A. Grzybowski in the Departments of Chemistry and of Chemical and Biological Engineering at Northwestern University. His scientific interests focus on complex chemical systems with an emphasis on reaction-diffusion and reaction networks.

Kristiana Kandere-Grzybowska graduated in biology from the College of Saint Rose in 1998. She obtained her PhD in biochemistry from Tufts University in September 2003 (with T. C. Theoharides), which was followed by a postdoctoral fellowship at Northwestern University funded by the Department of Defense. She is currently a Research Assistant Professor with Prof. B. A. Grzybowski in the Departments of Chemistry and of Chemical and Biological Engineering at Northwestern University. Her research interests include intracellular/cytoskeleton dynamics and cell motility in defined geometric confines and in cancer.

Marta Byrska received her MSc in Biology from Jagiellonian University (Krakow, Poland) in 2007 with research conducted at the University of Chicago in the Department of Biochemistry and Molecular Biology. She is currently a graduate student with Prof. Bartosz A. Grzybowski at Northwestern University. Her research focuses on cell motility at the molecular level, in particular on the synchronization of actin filaments, microtubules, and focal adhesions during the migration of cancerous cells.

Bartosz A. Grzybowski graduated in chemistry from Yale University in 1995. He obtained his doctoral degree in physical chemistry from Harvard University in August 2000 (with G. M. Whitesides). In June 2003, he joined the Faculty of Northwestern University where he is now Burgess Professor of Physical Chemistry and Chemical Systems Engineering. His scientific interests include self-assembly in non-equilibrium/dynamic systems, complex chemical networks, nanostructured materials and nanobiology. He is a recipient of several accolades including the ACS Colloids Unilever, Gerhard Kanig Innovation and 2010 Soft Matter Awards. His first book "Chemistry in Motion: Reaction-Diffusion Systems for Micro- and Nanotechnology" was published by John Wiley & Sons in 2010.
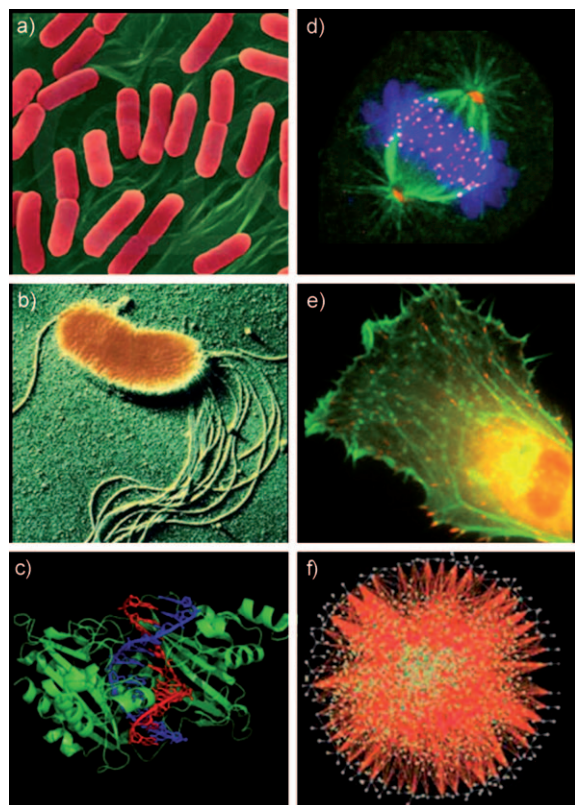
 Angew. Chem. Int. Ed. **2010**, *49*, 4170–4198

Figure 1. Examples of intracellular reaction-diffusion (RD) processes in prokaryotes (a–c) and eukaryotes (d,e). a) Selection of the cell center as a division site in *E. coli*; b) chemotactic motility of bacteria; c) targeting of specific sites on DNA by restriction enzymes; d) self-organization of mitotic spindle, e) eukaryotic cell motility; f) eukaryotic intracellular signaling. [Image credits: a) Copyright Dennis Kunkel Microscopy, Inc.; b) copyright Photoresearchers, Inc.; c) courtesy of RCSB PDB and from Ref. [292]; d) reprinted with permission from Prof. Harold Fisk from Ohio State University; e) reprinted with permission from Ref. [293]; and f) reprinted with permission from Ref. [294].]

it, analyze their pertinent scaling properties (characteristic times, dependencies on dimensionality, etc.), and review briefly the energetics of transport by RD in comparison to other possible modes of trafficking. We then discuss RD in prokaryotic cells. The examples we cover are chosen to allow comparisons with analogous processes in eukaryotes. The picture that emerges from this analysis leads us to suggest that RD—while certainly not the fastest way of moving macromolecules—might offer cells a favorable trade-off between delivery speed and energetic cost. If speed is not of essence, the cell can allow itself to use diffusion, which is "powered" by the always-present, "free-of-charge" thermal noise and does not consume the cell's energetic resources. On the other hand, if molecules need to be delivered to reaction sites rapidly and/or in a site-specific manner (such as in polarized secretion, or in the delivery of proteins to adhesion sites), the cell pays (in currencies such as ATP or GTP) extra energetic price for active transport. It is, essentially, the UPS Ground vs. FedEx situation, albeit on a cellular scale.

Another generalization we will attempt at the conclusion of our journey through cellular RD is that some "architec-

tures" of reaction-diffusion systems are conserved in different types of cells and phenomena. The fact that the same motifs are used over and over again suggests that biology optimized them to achieve desired functions. As such, these optimal motifs can be considered blueprints for man-made RD systems of the future that would mimic at least some biological functions. Before this vision materializes, however, we need to understand the basic principles that govern RD systems.

2. The Basics of Reaction-Diffusion Systems

Reaction-diffusion processes have been studied for over a century in both artificial and natural systems.[35,36] The former include oscillating Belousov–Zhabotinsky (BZ) and related reactions,[37–40] chemical waves in liquids,[41–43] in gels,[44,45] or on catalytic surfaces,[46,47] Liesegang rings[48–50] and other periodic precipitation patterns,[51,52] and discharge filaments.[53,54] In nature, RD gives rise to the layered texture of agates,[55] sculpts cave stalactites,[56] and determines the growth of dendritic limestones.[57] RD underlies a diverse range of biological phenomena including bacterial colonies,[58,59] cardiac activity,[60,61] and skin patterns.[62,63]

Reaction diffusion is a process in which the reacting molecules move through space as a result of diffusion. This definition explicitly excludes other modes of transport (drift, convection, etc.) that might arise from the presence of externally imposed fields and more "exotic" variants of diffusion, such as fractional diffusion (for example, subdiffusion or superdiffusion; see Refs. [64–66] for a more thorough review).

Diffusive transport is powered by thermal noise and gives rise to a flux that is proportional to the local concentration gradient. In one dimension, the diffusive flux (that is, the number of molecules diffusing through a unit cross-sectional area per unit time) is given by $\vec{j}(x,t) = -D\partial c(x,t)/\partial x$, where D stands for the diffusion coefficient. In three dimensions, $\vec{j}(x,y,z,t) = -D\nabla c(x,y,z,t)$, which is known as Fick's first law of diffusion (∇ is the gradient operator). Since diffusion conserves the number of molecules, the net diffusive flux into any small element of space is equal to the change of concentration within this element (Figure 2a). For a one-dimensional case, one can easily show that this is synonymous with $\partial(\vec{j}(x,t))/\partial x + \partial c(x,t)/\partial t = 0$; with the help of Fick's law, $\partial c(x,t)/\partial t = D\partial^2 c(x,t)/\partial x^2$ (assuming constant D). This result generalizes in three dimensions as $\partial c(\vec{r},t)/\partial t = D\nabla^2 c(\vec{r},t)$, where $\vec{r}$ is a position vector.

When a reaction occurs within an element of space, molecules of one or more type can be created or consumed according to specific reaction kinetics (Figure 2b). These events "add" to the diffusion equation and lead to RD equations of the general form $\partial c_i/\partial t = D_i\nabla^2 c_i + R_i(\{c_j\},t)$, where i denotes molecules of a specific type, $\{c_j\}$ is a set of concentrations on which the reaction term R_i depends, and dependencies of c_i on time and position are omitted to simplify the notation. For example, for a simple case of one type (A) of molecule diffusing and reacting according to $dc_A/dt = -kc_A$, the RD equation is $\partial c_A/\partial t = D_A\nabla^2 c_A - kc_A$.
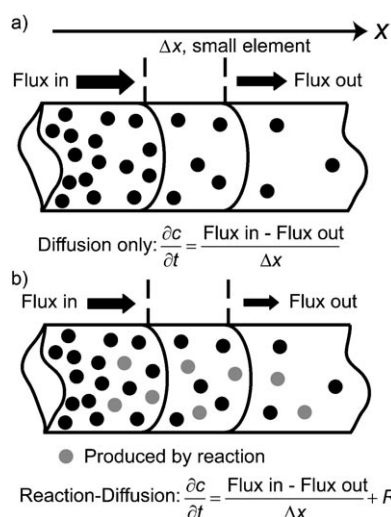
Figure 2. a) Diffusion and b) reaction diffusion in a one-dimensional system (here, a thin circular tube).

In general: 1) As many equations are necessary to describe a RD system as there are types of molecules whose concentrations change in space and/or in time and 2) the complexity of the system increases rapidly if the equations are coupled to one another by autocatalysis or feedback. An illustrative example here is that of a system involving only two types of intermediates, A (activator) and S (substrate), whose concentrations change according to the autocatalytic reaction $2A + S \xrightarrow{k_1} 3A$, the "decomposition" reaction $A \xrightarrow{k_2} P$, and the "production" reaction $R \xrightarrow{k_3} S$ (see Figure 3a). Since reactant R is assumed to be in excess, its concentration can be approximated as constant, and two equations are needed to describe the reaction and diffusion phenomena in this system [Eqs. (1) and (2)].

$$\frac{\partial c_A}{\partial t} = D_A \nabla^2 c_A + k_1 c_A^2 c_S - k_2 c_A \tag{1}$$

$$\frac{\partial c_S}{\partial t} = D_S \nabla^2 c_S - k_1 c_A^2 c_S + k_3 \tag{2}$$

Here, D_A and D_S are the diffusion coefficients of A and S, respectively, and k_1, k_2, and k_3 are the reaction rate constants. When diffusion of the substrate S is significantly faster than that of the activating species A (that is, $D_S \gg D_A$), this RD system can display a variety of intricate spatial patterns (so-called Turing patterns, after their discoverer, Alan Turing[67]) that result from an interplay between local aggregation of A through autocatalysis and rapid diffusion of S away from A-rich regions. Interestingly, the examples of Turing patterns modeled in Figure 3 are also observed in several biological systems, including zebras (stripes), minor worker termites[68,69] (concentric circles), aggregation of slime molds[70] (spirals), and leopards (randomly distributed dots).

2.1. Limiting Cases and Characteristic Times

The RD equations are usually difficult to solve, and for all but the simplest cases require the use of advanced numerical
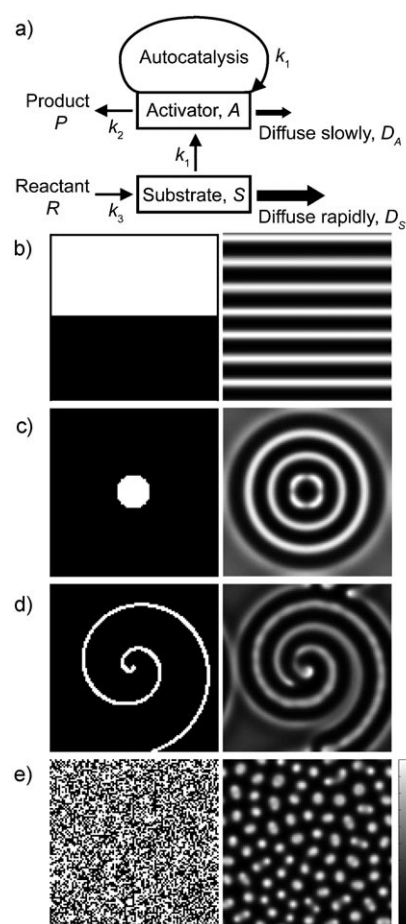

Figure 3. Examples of pattern formation in a Turing-type RD system. a) Reaction scheme in which reactant R produces substrate S, which in turn contributes to the autocatalytic production of A. The local aggregation of A is made possible by the combination of autocatalysis with the low diffusivity of A. b–e) Different initial distributions of A (left column) produce different types of RD patterns (right column). Parameters used in the simulations were $D_A = 1 \times 10^{-8}$ cm²s⁻¹, $D_S = 2 \times 10^{-7}$ cm²s⁻¹, $k_1 = 1$ M⁻² s⁻¹, $k_2 = 1$ s⁻¹, and $k_3 = 1$ M s⁻¹. The size of the domain is 100 μm × 100 μm (represented in the simulations as a 100 × 100 grid), with periodic boundary conditions imposed. Simulations were run for 20 s at a time step of 0.01 s. For all the patterns, white represents a high concentration and black represents a low concentration of A.

methods.[71] Even without all the mathematical nuances, however, one can get a good "feel" for the main characteristics of RD processes. First, there are two limiting cases for reaction-diffusion systems. If the reactions are much slower than the diffusion of species ("reaction-limited" case), the RD equations can be approximated as $\partial c_i/\partial t = R_i(c_i, t)$; if they are much faster ("diffusion limited"), one can write $\partial c_i/\partial t = D_i \nabla^2 c_i$. In general, the relative speeds of reaction and diffusion can be estimated by the order-of-magnitude of the "characteristic times". For reactions, the characteristic times are related to the reaction rates (namely, $\tau_{i,R} \sim 1/k_i$ for species i reacting according to the first-order kinetics). For diffusion, the characteristic time τ_D is the time it takes a molecule/object to diffuse some characteristic distance L over which the processes of interest take place (that is, $L \approx 1$ μm

for RD in a prokaryotic cell[34] and $L \approx 30\ \mu m$ for a typical eukaryote[34]). Making order-of-magnitude approximations to the terms in the diffusion equation gives $\partial c/\partial t \sim c/\tau_D$ and $D\partial^2 c/\partial x^2 \sim Dc/L^2$, and equating these estimates gives $\tau_D \sim L^2/D$ (the same result can be derived from the well-known linear relationship between the mean-square distance traveled by a diffusing particle and time). For example, for the diffusion of GFP through an *Escherichia coli* bacterium ($L \approx 1\ \mu m$ and diffusion coefficient[72] $D \approx 7.7 \times 10^{-8}\ cm^2 s^{-1}$), the characteristic time is $\tau_D \approx 0.1\ s$. For an analogous process taking place in a larger, eukaryotic cell ($L \approx 30\ \mu m$, diffusion coefficient[73] $D \approx 8.7 \times 10^{-7}\ cm^2 s^{-1}$) this time is about two orders of magnitude longer ($\tau_D \approx 10\ s$).

A dimensionless number $Da = \tau_D/\tau_R$ that expresses the ratio of the characteristic diffusion and reaction times is known as the Damköhler number and tells us whether the process is reaction-limited ($Da \ll 1$), diffusion-limited ($Da \gg 1$), or whether both reaction and diffusion need to be considered and full RD equations tackled ($Da \approx 1$). Not surprisingly, the most interesting and rich phenomena are observed in the $Da \approx 1$ regime, which will be the case for the majority of the cellular systems considered here.

2.2. Dimensionality

The second point concerns dimensionality and the average times needed for diffusing particles to find their reaction partners. Intuitively, one would expect that if a particle has to find a reaction partner at some specific location and distance L it will do so more rapidly if it is constrained to a one-dimensional manifold (that is, a line) rather than being able to wander freely over a 2D plane or 3D space. In the context of cells, an instructive example is that of a domain of radius L enclosing a "nucleus" of radius $a \ll L$ with the concentration of the diffusing molecules initially uniform outside of the nucleus (Figure 4). For this configuration, one can define the so-called arrival time τ_A, that is, the average time it takes a molecule in the cell to reach its target in the nucleus. By following calculations detailed in the Supporting Information, it can be shown that Equations (3)–(5) hold for the one-dimensional [Eq. (3); "linear cell", Figure 4a], two-dimensional [Eq. (4); "pancake cell", Figure 4b], and three-dimensional cases [Eq. (5); "spherical cell", Figure 4c].

$$\tau_A \approx L^2/3D \qquad (3)$$

$$\tau_A \approx (L^2/2D)\ln(L/a) \qquad (4)$$

$$\tau_A \approx (L^2/3D)(L/a) \qquad (5)$$

Figure 4d shows that for a given a and for varying L, the 1D and 2D times are comparable but markedly smaller than for the 3D case. The practical consequence of these considerations is that the rate of the diffusive delivery can be increased by reducing the dimensionality of the system. An important manifestation of this behavior is shown in Section 3.3 when we discuss the targeting of specific DNA sites by proteins that prefer to "slide" along the (1D) DNA strand
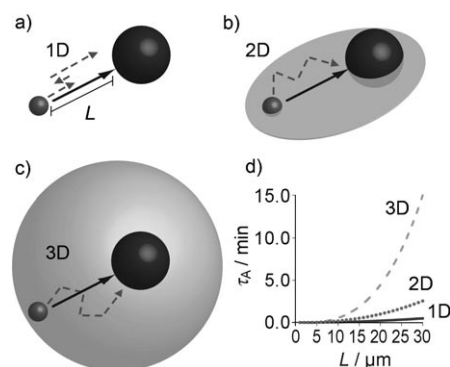

Figure 4. The dimensionality affects the effectiveness of diffusive transport. Molecules (left, smaller spheres) reach reaction targets (right, larger spheres) at distance L by diffusing a) along one-dimensional/linear trajectory; b) over a two-dimensional plane, and c) through a three-dimensional space. The gray dashed curves give "realistic" trajectories. The black solid arrows give, for comparison, the shortest trajectory possible. The plot in (d) gives the average arrival times as a function of the domain size for one- (solid curve), two- (dotted curve), and three-dimensional (dashed curve) cases. The arrival times increase with dimensionality: The 3D time is significantly longer than in either the 2D or 1D cases. The parameters used to generate these plots are $D = 1 \times 10^{-7}\ cm^2 s^{-1}$ and $a = 1\ \mu m$.

rather than find these sites by moving freely in 3D space. Another example (see Section 4.1.1) is cell motility, where flattening of a cell spread on a substrate effectively accelerates the diffusion of molecules involved in signaling (for example, GTPases and phosphoproteins) toward intracellular targets (for example, in the nucleus) compared to the same cell in a three-dimensional, non-adherent state.[74] In this case, the time of the signal propagation is determined by the length of the shortest diffusive path, which is smaller along the short axis of a flattened, "pancake" cell than along any direction of a non-adherent, "spherical" cell.

2.3. Energetics and Efficiency of Cellular RD

Since cells operate outside of thermodynamic equilibrium, they need a constant supply of energy to maintain a range of vital functions, of which transporting molecules across the cell is only one. Let us first examine what would be the consequence if all transport routes were active (namely, powered by the high-energy molecules such as ATP, GTP, or NADH). As an example, consider the transport of a secretory vesicle along microtubules, which is driven by kinesin motor proteins and is "fueled" by ATP (other organelles such as mitochondria or Golgi apparatus can also be transported along microtubules or microfilaments[75]). The speed of kinesin on a microtubule is about $3\ \mu m s^{-1}$ and a single step is roughly $8\ nm$[75,76]—therefore, this motor protein makes around 375 steps per second, with each step requiring the consumption of one ATP molecule. Given that about 1000 secretory vesicles are transported on microtubules of an eukaryotic cell at every instant of time,[77,78] the total rate of energy consumption as a result of vesicle transport is approximately 3.75×10^5 ATP molecules per second. On the

other hand, since the total number of ATP molecules in a cell at any given moment is about 10^9,[75,79] and since these molecules are used up and completely replaced in roughly 1–2 min,[75] the total rate of consumption by the cells is approximately 10^7 ATP molecules per second. It follows that the kinesin-on-microtubule motors use as much as about 4% of the cell's ATP fuel by transporting 1000 vesicles. Moreover, this number is only a very conservative lower boundary, and would be much higher if the cell indiscriminately moved all its contents by this energy-costly mechanism. For example, if yeasts decided to transport all their 15 000 proteins[80] actively, they would have to allocate about 60% of their total energetic resources to the task, thus leaving very little room for all other vital functions.

In sharp contrast, diffusion is "free of energetic charge", as long as the gradients of concentrations are sustained—we will see in subsequent sections that such gradients are inherent to the functioning of a cell, where molecules are being synthesized and consumed at different loci. Under in vivo conditions, the molecules within a concentration gradient are "jiggled" by random Brownian motions which, as can be shown by elementary statistical considerations, give rise to a net flux/transport of these molecules from the regions of high to the regions of low concentration. Again, this transport itself does not require additional expenditure of energy.

With the energetic considerations corroborating the need for passive transport, let us briefly revisit the question of the delivery speed. In this context, it might come as a bit of a surprise that, depending on the size of the cargo, the "UPS Ground" diffusive delivery might actually be as efficient as the "FedEx" active transport. This is illustrated in Figure 5, in which the characteristic times of diffusive delivery of 3, 10, and 20 nm spherical cargos are plotted against distance L, and these times are compared with the time of delivery by microtubules. While diffusion is significantly slower than active transport for large cargos, the two modes of transportation become comparable for particles with a diameter of about 3 nm. This finding suggests that in the case of small macromolecules, the cell should either "package" these entities into larger vesicles prior to "shipment" on microtubule/microfilament tracks or, if the molecules are to be transported individually, should be able to rely on diffusive delivery instead of energetically more costly active transport. This is indeed the case, and only a few macromolecules/proteins (for example, p53, neurofilament protein, APC protein[81–83]) are actively moved on microtubules. Arguably the most important example is the p53 protein, which is involved in cell-cycle control, apoptosis, differentiation, DNA repair and recombination, as well as centrosome duplication, and is transported on microtubules by dynein.[81] This protein, however, is significantly larger (ca. 50 nm in diameter for the p53 tetramer[81,84]) than typical proteins, and its transport by diffusion would be 25 times slower than delivery on microtubules over a distance of 5 μm.

In summary, passive/diffusive intracellular transport is favored by several factors: 1) the limited amount of energy deployable for active transport on filamentous "tracks"; 2) the distance over which the transport is to take place (the
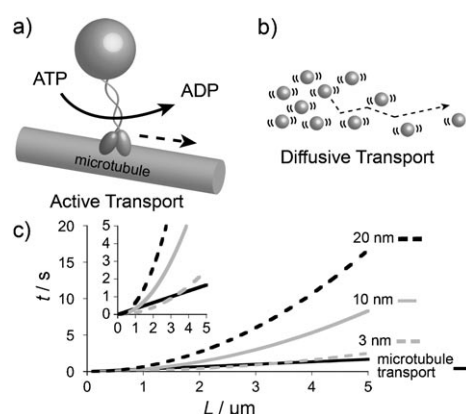

Figure 5. Comparison of active and diffusive transport. a) Scheme illustrating active transport (here, kinesin on a microtubule) requiring consumption of ATP, and b) diffusive transport driven by "free of charge" random thermal motion (denoted by the "halos" around the particles). c) Times needed to transport nanometer-sized cargos either by the use of microtubules (black curve) or by diffusive transport for 3 nm (gray dashed curve), 10 nm (gray curve), and 20 nm (black dashed curve) cargos. The time needed for a 3 nm diameter particle to diffuse is similar to the time needed to transport the same particle on a microtubule. However, the diffusive times are much longer for larger cargos. The plot was generated using the $t \sim L^2/D$ scaling with the diffusion coefficient of a typical 3 nm protein $D \approx 1 \times 10^{-7}$ cm^2 s^{-1} and the diffusion coefficients of larger particles approximated from the Stokes–Einstein relationship $D = kT/3\pi\mu(2R_p)$ (where $2R_p$ is the particle diameter). The inset shows a magnification of the first five seconds of the main plot.

larger this distance, the less efficient the diffusive delivery); and 3) the size of the cargo (the smaller it is, the faster its diffusion).

With these general considerations, let us now examine specific situations in which diffusive delivery is coupled with biochemical reactions to set up RD systems in prokaryotes and in eukaryotes.

3. RD in Prokaryotes

In the "primitive" prokaryotic cells, active transport mechanisms are rare (save few exceptions such as segregation of two plasmid DNA clusters by a pushing force generated by the polymerization of bacterial actin homolog ParM,[85–88] or chromosomes partitioning under the pulling force generated by ParA proteins[89–92]) and substrates are usually delivered to the reaction sites by diffusion. For most intracellular processes, the characteristic diffusion times are on the order of 0.1 s and significantly longer than the reaction times—consequently, such processes are diffusion-limited (Da ⩾ 1 see Section 2.1). For some essential cellular functions, however, both diffusion and reaction occur on commensurate time scales. In this Section we discuss the most prominent examples of such RD systems—cell signaling, chemotaxis, cell division, and recognition of target sites on DNA. These examples allow for direct comparisons with analogous processes in eukaryotic cells we will cover later.

3.1. Prokaryotic Signaling Systems and Chemotaxis

Many signaling pathways in bacteria are two-component systems based on the phosphorylation of two key effector proteins.[93,94] The primary protein involved in signal transduction is a membrane-bound sensor histidine kinase which comprises an extracellular specific input domain (detecting specific environmental signals) coupled to an autokinase domain. The second component of this signaling system is a cytosolic regulator domain, which triggers cellular response. After binding of an extracellular ligand to the input domain, the histidine kinase autophosphorylates and subsequently transfers the phosphoryl group to the receiver domain of the cytosolic response regulator. The phosphorylated response regulator then diffuses across the cell and reacts with its target, which subsequently initiates cellular response.

Chemotactic motility of bacterial cells[95] is an example of a process based on a two-component signaling system in which RD orchestrates signal transduction (Figure 6). Bac-
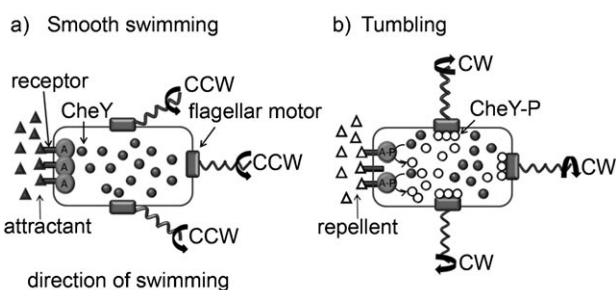

Figure 6. Two-component RD signaling system in chemotactic bacterial cell motility. Bacteria exhibit two different swimming patterns depending on the direction of rotation of the flagellar motor. Counterclockwise (CCW) rotation results in smooth bacterial swimming, whereas clockwise (CW) rotation causes bacterial tumbling. a) When surface receptors bind attractant molecules (solid triangles), autophosphorylation of the CheA kinase (denoted as A) is inhibited and CheY remains inactive (unphosphorylated) while diffusing through the cytoplasm (solid circles). The flagella rotate CCW, which results in the formation of a stable flagellar bundle and in smooth swimming in the direction of increasing attractant concentration. b) When, however, surface receptors bind the repellent molecules (open triangles), CheA autophosphorylates (A-P) and subsequently phosphorylates/activates CheY. Phosphorylated CheY (CheY-P, open circles) then diffuses to the flagella where it reacts with motor proteins, changing the direction of the flagella's rotation to CW, which in turn results in bacterial tumbling.

teria exhibit two different swimming patterns depending on the direction of flagellar motor movement. Counterclockwise (CCW) rotation causes flagella to assemble into a stable bundle and results in forward swimming (commonly referred to as smooth swimming). Clockwise (CW) rotation separates the flagellar bundle and causes bacterial tumbling (chaotic motion).[96] The direction of flagellar rotation is regulated by a two-component signaling system between receptor-CheA kinase-CheW complex and CheY protein, which diffuses in response to the presence of the stimulus (attractant/repellent) gradient. Clusters of receptor-CheA kinase-CheW complexes are localized preferentially in the membrane at the poles of the cell[97] where they sense the presence of attractants/repellents in the outside environment and change the phosphorylation status of the intracellular CheY protein. The binding of repellents to specific receptors on the cell surface results in autophosphorylation of CheA, which, in turn, leads to the phosphorylation/activation of CheY. Phosphorylated CheY (CheY-P) diffuses to the flagella where it reacts with motor proteins, thereby changing the direction of the flagella's rotation to CW and leading to bacterial tumbling (Figure 6). In contrast, binding of attractants to the receptor prevents autophosphorylation of CheA and activation of CheY—consequently, the bacterium swims straight toward the increasing concentration of attractant. In these processes, the response time of the flagella—that is, the time required for CheY to diffuse from the receptor site to the motor and to subsequently associate with this motor—has been measured experimentally to be 50–200 ms.[98,99] These values are close to the theoretical estimate of the characteristic time for the two-dimensional diffusion of $\tau_D \sim L^2/D$, which for the diffusion of a small protein such as CheY through the cytoplasm is 100 ms (assuming $L = 1$ μm and the diffusion coefficient $D = 1 \times 10^{-7}$ cm^{2}s^{-1} for CheY[72,100]). The rate constant for the CheY–motor association is $k \approx 3 \times 10^6$ M^{-1}s^{-1}[101,102] and the average concentration of CheY in the cell is approximately 3 μм,[103] which gives the characteristic reaction times ($\tau_R \sim 1/kc_{CheY}$ for species reacting according to a second-order kinetics) for CheY–motor association also on the order of 100 ms. It follows that the Damköhler number Da $= \tau_D/\tau_R$ for the process is on the order of unity. Thus, based on the arguments from Section 2.1, signal transduction in bacterial chemotaxis is a RD process. Other accompanying processes such as the initial chemoreceptor–ligand interactions are assumed to be fast[98] compared to the processes already described, which is why they do not have to be taken into account in the above analysis. Interestingly, the dynamic behavior of molecules involved in chemotaxis has been simulated by using a discrete, stochastic version of the reaction diffusion system, with the program called "Smoldyn" (for Smoluchowski dynamics);[104] the modeled response times of the flagella (100–300 ms) were found to be in agreement with the experimental data.

An additional reason that justifies the "choice" of RD to mediate chemotactic response is that it allows the CheY diffusing through the cytoplasm to be modified/dephosphorylated by other "signals", such as the cytoplasmic CheZ protein. Such modifications allow cross-talk and adaptation[105,106] of the cell to external signals. This can be illustrated for the case when a cell starts detecting a repellent whose concentration gradually equalizes around the cell. Initially, upon detection of the repellent's gradient, CheY is phosphorylated, diffuses to the flagella, and causes the cell to tumble rather than to swim forward. However, after the concentration of the repellent equalizes, it is important for the cell to maintain some ability to continue its random walk in search of an attractant (and "food"). This is achieved through the action of CheZ, which rapidly[107] dephosphorylates CheY-P, thereby allowing the cell to swim and "escape" the region saturated by the repellent. If the CheY transport were active

(for example, mediated by cytoskeletal fibers such as in the eukaryotes), this kind of cross-talk would be impossible (unless the CheY cargo were periodically "unloaded" from the transporter), thus limiting the ability of the cell to respond to the CheZ regulatory signals.

3.2. The Oscillating Min System in Bacterial Cell Division

The next prominent example of RD in prokaryotes is cell division, where a subtle interplay between reaction and diffusion helps define and select the cell's center as a division site. Before division occurs, the cell first grows in size and then replicates and segregates its duplicated chromosomes (each bacterial cell has one chromosome that before cell division duplicates into two). This segregation process starts with the formation of a contractile polymeric "Z ring" of a tubulin-homologue FtsZ just underneath the cytoplasmic membrane.[108] The accurate positioning of the "Z ring" in the middle of the cell is crucial for the ultimately even distribution of the chromosomes in the daughter cells. Experiments show that wild-type *E. coli* locates the plane of division with a remarkably high precision of $(50 \pm 1.3)\%$ of the cell's length.[109] Numerous studies[110–115] indicate that this precise positioning derives from RD process involving the so-called Min proteins (MinC, MinD, and MinE; see Figure 7) oscillating between the cell's poles (the longest axis of the cell) with a period of approximately 1–2 minutes.[116] If the Min system is genetically knocked out, 40% of cell divisions lead to the production of nucleoid-free minicells, whereby lopsided division fails to incorporate the chromosome in these cells.[110]

MinD is an ATPase that dimerizes in the presence of ATP (Figure 7a). This dimerization process exposes amphiphilic helices on the MinD protein and enables the hydrophobic portions of these proteins to bind to the cell membrane.[117] Importantly, MinD dimers form over only half of the cell. Next, MinE binds to membrane-bound MinD and induces the hydrolysis of ATP by MinD. Subsequently, both proteins, MinD:ADP and MinE, detach from the membrane. Released MinD:ADP then diffuses to the other cell pole, undergoes ADP/ATP exchange and dimerization, which is then followed by reassembly on the membrane of the opposite half of the cell. During this time, MinC simply follows the movement of MinD and does not have any effect on the interactions between MinD and MinE. However, the essential function played by MinC is preventing the assembly of the contractile "Z ring".[118] As a consequence of inhibiting the formation of the "Z ring" at the cell poles, the Min system directs the division site to be formed exactly at the middle of the cell.[110–115]

Let us separate this complex sequence of events into the key components of the underlying RD process. First, we recognize that the most important phenomenon involved is the harboring of the MinD protein to only half on the cell membrane—when, subsequently, the "halves" oscillate between the cell's poles, the position of the Z ring is naturally defined. The question to answer is then how the MinD proteins evolve from the initial, uniform distribution within the cell to the asymmetric, half-of-the-cell one. This so-called
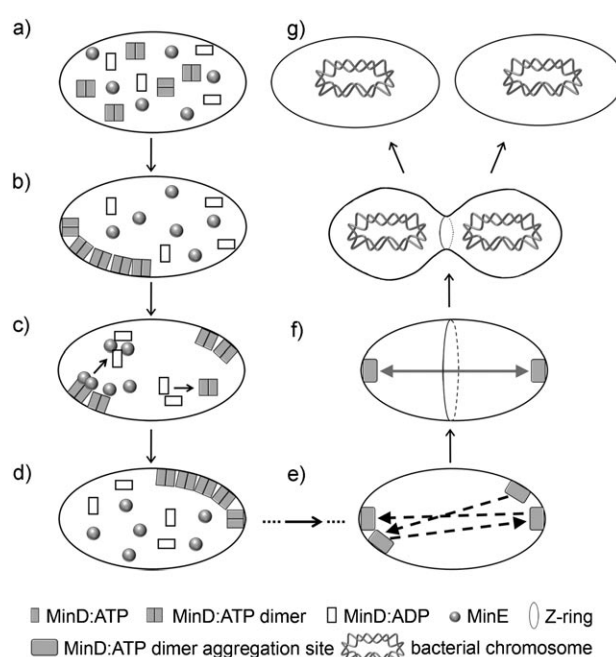

Figure 7. Oscillations of the Min system direct the formation of the Z ring and division of bacterial cells. a) Initially, Min proteins are homogeneously distributed throughout the cell. b) Small, stochastic concentration variations lead to more MinD:ATP binding and aggregation at a certain region of the membrane. c) After the aggregation site is formed, MinE induces hydrolysis of MinD-bound ATP to ADP, which causes the release of MinD from the membrane into the cytoplasm. MinD:ADP is "recharged" to MinD:ATP while diffusing through the cytoplasm. Since the original site is still consuming MinD:ATP, the concentration of MinD:ATP is highest furthest away (approximately "diagonal") from the original site, where the new aggregation event commences. d) The aggregate grows autocatalytically at this new aggregation site. e) The "bouncing" of the aggregation site continues until the oscillation locks along the longest axis of the cell. f) In this stable oscillation cycle, the aggregation sites alternate between the poles of the cell. MinC (not shown) follows the movement of MinD and inhibits the formation of the so-called Z ring, which defines the plane of cell division. g) The cell ultimately divides at the cell center, where the time-averaged concentration of MinC is lowest. The bacterial cell is in reality rod-shaped, but it is shown here as an oval to simplify the illustration.

symmetry-breaking event can be explained by a combination of autocatalytic reaction and diffusion of species. Specifically, when free MinD:ATP dimers bind to the membrane, the binding rate is higher at locations where the concentration of the product (that is, membrane-bound MinD:ATP) is also high. The kinetic equation for MinD:ATP at the membrane can be written as Equation (6), where k_n are reaction rate constants, c_A denotes the concentration of membrane-bound MinD:ATP (autocatalytic!), c_B the concentration of the membrane-bound MinD:MinE:ATP complex (for which $\partial c_B / \partial t = k_3 c_A c_E - k_5 c_B$), c_C is the concentration of the free MinD:ATP throughout the cell (that is, not only near the membrane), and c_E is the concentration of the free MinE, which induces dissociation of the complex from the membrane (hence, the minus sign before the second term).

$$\frac{\partial c_A}{\partial t} = [k_1 + k_2(c_A + c_B)]c_C - k_3 c_A c_E \qquad (6)$$

Of course, this kinetic equation is coupled to the diffusion of the free Min (both its ATP and ADP forms). The RD Equations (7) and (8) account for the changes in the concentration of free Min.

$$\frac{\partial c_C}{\partial t} = D_C \nabla^2 c_C + k_4 c_D - \delta(r - R)[k_1 + k_2(c_A + c_B)]c_C \tag{7}$$

$$\frac{\partial c_D}{\partial t} = D_D \nabla^2 c_D - k_4 c_D + \delta(r - R)k_5 c_B \tag{8}$$

Here, c_D denotes the concentration of free MinD:ADP, D_C and D_D are the diffusion coefficients of free MinD:ATP and MinD:ADP, respectively, k_4 is the reaction rate constant for nucleotide exchange (when MinD:ADP is converted into MinD:ATP), and k_5 is the rate constant of detachment of MinD:ADP from the membrane to the cytoplasm. The delta function $\delta(r-R)$ specifies the location at which the reaction takes place at the membrane (r is the spatial coordinate and R the specific location at the membrane). Since the region of MinD:ATP aggregation is also the site of consumption of the MinE proteins, the concentration of MinE proteins therein is low. Consequently, the remaining, free MinE proteins diffuse down the concentration gradient, further disintegrating the MinD:ATP aggregates. In terms of RD equations, this process can be quantified by Equation (9), where D_E is the diffusion coefficient of free MinE protein.

$$\frac{\partial c_E}{\partial t} = D_E \nabla^2 c_E - \delta(r - R)k_3 c_A c_E + \delta(r - R)k_5 c_B \tag{9}$$

When these equations are solved numerically (for details, see Ref. [114]) starting from the spatially uniform initial distribution (with infinitesimally small random noise) of all species, they reproduce the symmetry breaking and subsequent Min oscillations. While numerical details are beyond the scope of this Review, the sequence of events these equations entail can be qualitatively narrated as follows (see Figure 7). First, any small disturbance in the initial concentration of MinD:ATP—in reality because of thermal noise, which in computer simulations is mimicked by the imposed initial conditions—is amplified by the autocatalytic term in Equation (6). As the MinD:ATP aggregation sites form, MinE starts dissociating them, thereby liberating MinD:ADP into the cytoplasm. Before being able to rebind to the membrane, however, MinD:ADP needs to be "recharged" back to MinD:ATP. During this recharging, MinD:ADP diffuses throughout the cytoplasm and establishes a concentration gradient of MinD:ATP (low concentration near the aggregation site; high concentrations farthest away from the site). When an excess of MinE finally disintegrates the original aggregation site, the new site is most likely to form at the farthest region, "diagonally" across the cell, where there is most newly "recharged" MinD:ATP (Figure 7c,d). When this billiard-like process repeats many times, the stable configuration is ultimately reached, where the "farthest" sites are at the poles along the cell's longest axis. The aggregation sites then oscillate between the two poles, thereby resulting in a low net concentration of MinD protein (and, consequently, of the MinC protein) at the "middle" of the cell (see Figure 7 f).

Since MinC inhibits the assembly of the "Z ring", this ring forms along the cell's "equator". When this happens, the duplicated chromosomes are separated, thus leaving a nucleoid-free region in the cell's middle. Components necessary for the formation of the cell wall are also recruited, thereby enabling the "Z ring" to contract and constrict and, ultimately, to divide the cell into two progenies, each containing complete chromosome.[119] For further comments on the model's performance, see Ref. [120].

3.3. Targeting of Specific Sites on DNA by Proteins

The targeting of specific sites on DNA by proteins underlies a range of important cellular events,[121,122] and is yet another example of a reaction-diffusion system in prokaryotic cells. This targeting process has long been a topic of intense discussion and even controversy,[121,123–125] stemming from the fact that the experimentally measured times required for proteins to reach specific target sites on DNA[121] are one to two orders of magnitude shorter than theoretical predictions for 3D diffusion. The first observation of this discrepancy was reported in 1970 for bacterial LacI repressor, which binds to its target within the *lac* operon about 100 times faster than the 3D diffusion limit.[126,127] In this Section, we will discuss two experimentally verified mechanisms[128–130] of DNA target site localization, in which the combination of reaction (namely, binding to DNA) and diffusion (sometimes modified by the spatial fluctuations of the DNA) offers a significant decrease in the localization times—as compared to "random" diffusive targeting[124,125] in three dimensions—by effectively reducing the dimensionality of the targeting process.

3.3.1. Sliding

The first mechanism, called sliding, is based on the presence of nonspecific DNA binding sites that flank the target site.[128] Since specific target sites are short (nanometers) and sparsely distributed[127,128] on long (micrometer) DNA[126,128] strands, a randomly diffusing protein is much more likely to first encounter a nonspecific DNA region. However, as the nonspecific binding is weak, the protein can diffuse or "slide" along the DNA toward the target site (Figure 8a). Based on the argument from Section 2.2, the targeting time for random 3D diffusion toward a site of size $a \approx 1$ nm is roughly $\tau_A \approx (L^2/3D_3)(L/a)$, which for typical parameters that characterize diffusion in a prokaryotic cell (diffusive length $L \approx 1$ μm, 3D diffusion coefficient $D_3 \approx 1 \times 10^{-7}$ cm^{2}s^{-1}) is about 33 s. In contrast, for the "sliding" 1D diffusion along DNA, $\tau_A \approx L^2/3D_1$, which for a typical experimentally estimated 1D diffusion coefficient $D_1 \approx 1 \times 10^{-9}$ cm^{2}s^{-1},[128,131] gives a targeting time of only around 3.3 s. This conservative estimate shows that 1D diffusion is at least an order of magnitude faster than 3D diffusion (see Halford and Marko[127] and Wang et al.[128] for a more detailed discussion). One classic example of a protein that targets the DNA site by the sliding mechanism is the already mentioned LacI repressor.[126] This particular sliding has been thoroughly
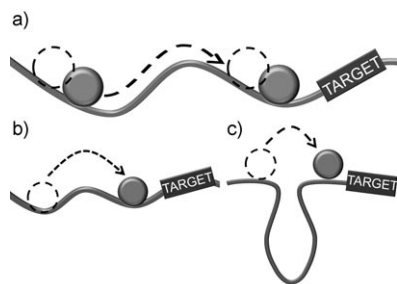
Figure 8. The reduction of the effective dimensionality of protein diffusion accelerates the localization of proteins onto DNA target loci. The picture illustrates three targeting mechanisms: a) sliding, b) hopping, c) jumping. See Section 3.3 for details.

studied by fusing a GFP protein to the LacI repressor and using total internal reflection fluorescence microscopy (TIRFM) to observe the single fluorescent molecule performing 1D Brownian motion on DNA strands.[128,132]

3.3.2. Hopping and Jumping

The second mode of accelerated targeting is by "hopping/jumping". In this process, a protein occasionally dissociates from DNA and rebinds at a site away from the initial one.[129] Sometimes this new binding locus is only a few base pairs away from the previous one ("hopping",[125,133] Figure 8b), but there are also cases when the folding of a DNA strand makes the sites that are hundreds of base pairs apart proximal in space—in such cases, the protein does not need to slide a long distance but can rather perform a "jump"[125] (Figure 8c).[134]

Experiments[129,135,136] have shown that proteins typically both slide and hop/jump when searching for their targets on DNA. This combination changes the nature of the motion from a purely Brownian walk to a so-called Lévy flight, which is known to be the optimal searching strategy in numerous biological systems,[137–140] especially when the domain to be searched is much larger than the target itself. Mathematically, Lévy flight is characterized by an algebraic probability distribution P of making a step of length l, $P(l)=l^{-\mu}$. In this expression, μ is a constant in the range $1<\mu\leq3$—the larger this exponent, the more biased the flight toward smaller steps and more diffusion-like the process. Indeed, when $\mu=3$, Lévy flight reduces to the Brownian random walk; when $\mu=1$, the process is dominated by long jumps. Not surprisingly, there is compelling evidence[137,141] that the optimum strategy for searching the target on DNA corresponds to the middle-of-the-way situation ($\mu=2$), when longer jumps help the proteins to explore space while local Brownian "jiggles" allow for precise localization on a nearby target. It has also been confirmed experimentally[129,136,142] that both sliding and hopping/jumping are operative in vitro at ionic strengths comparable to in vivo conditions. Interestingly, sliding is the preferred mechanism at low salt concentrations, whereas hopping/jumping dominates at higher concentrations. One possible explanation is that the salt ions screen and weaken the electrostatic DNA–protein attraction,[274] thus facilitating protein detachment from DNA and promoting hopping/jumping. The efficiency of the jumping mechanism has also been further demonstrated by experiments in which optical tweezers were used to manipulate DNA strands from naturally coiled to fully extended configurations.[130] It was found that the targeting rate in the coiled state (where jumping is operative) was twice that observed in the fully extended state (where jumping is efficiently eliminated).

4. RD in Eukaryotes

Serial symbiotic events of ancient bacteria,[143,144] which occurred during evolution and gave rise to eukaryotic cells, were milestones in the evolution of life.[145] Eukaryotic cells are significantly larger than prokaryotic ones (typically 10–30 μm in diameter versus ca. 1 μm), and consist of an intracellular cytomembrane network (including the rough endoplasmic reticulum, ER, the related nuclear envelope, the smooth ER, the Golgi complex, endosomes, and lysosomes), the cytoskeleton, and genetic material inside the nucleus.[146,147]

As we have argued in Section 2.3, the larger size of eukaryotes favors the active modes of transport of large membrane-bounded vesicles, cellular organelles, mRNAs, and proteins along well-defined cytoskeletal tracks (predominantly microtubules, but also actin filaments). In most cells, microtubules are polarized with their minus ends directed toward the nucleus and the plus ends pointing toward the cell periphery. Intracellular transport along microtubules is mediated by cytosolic motor proteins—the kinesins, which are plus-end directed, and the dyneins, which are minus-end directed. These motor proteins bound to their cargos (for example, vesicles) and tracks (microtubules) utilize ATP as a source of energy. The polarized nature of microtubule tracks enables site-directed delivery, such as polarized secretion, maintenance of apico-basal polarity, and sorting of molecules to two distinct ends of apico-basally polarized cells.[34]

Active transport is efficient for large loads and indispensable for the delivery of "urgently needed" molecules. For example, the diffusion constant for a 100 nm vesicle (estimated through the Einstein–Stokes relationship, see Figure 5) through the cytosol is 0.3 μm²s, and delivering this vesicle from the cell membrane to the nucleus (about 5 μm) would take over 80 seconds. In contrast, active transport along microtubules offers a speed of around 3 μm s⁻¹[148] and a delivery time of only 1.7 seconds. In another example, mRNA sorting to defined subcellular compartments mediated by microtubular transport[149] is essential for localized protein synthesis, which is particularly critical for developing embryos[150–152] (where delocalized protein production could lead to serious defects) and also for most other types of cells.[153–158]

Although there are many more examples where active transport is rapid and efficient, it costs a lot of energy (see Section 2.3), and many important processes in eukaryotes still rely on diffusive delivery coupled with biochemical reactions. The examples we chose are intended to mirror as closely as possible those we covered in Section 3 for prokaryotes. In the following, we thus focus on RD processes that are operative in

cell signaling, those that underlie the organization of the mitotic spindle, and those that enable cell motility.

4.1. Signaling in Eukaryotic Cells
4.1.1. Signaling Pathways

Eukaryotic cell signaling is mediated by molecules arranged into pathways and governs/coordinates cellular responses to stimuli coming from the outside environment. The common motif of signaling pathways is typically composed of two forms of proteins that can be converted into one another by the action of two enzymes of "opposing" activities (Figure 10a), for example, protein kinase that phosphorylates other proteins (into the so-called phosphoproteins) and protein phosphatase responsible for dephosphorylation.[159]

Signal transduction starts at the cell membrane with the binding of a ligand to its cognate membrane receptor. This event results in activation of the receptor, which then activates cytoplasmic signaling proteins that ultimately transmit the signal to the nucleus where they trigger a cellular response, such as gene expression.

In the context of RD, the key observation is that kinases and phosphatases—that is, enzymes that activate/deactivate signaling proteins—are spatially separated in the cell. The receptor kinases are localized almost exclusively at the cell membrane, whereas phosphatases are often distributed uniformly throughout the cytoplasm. Consequently, phosphoproteins become phosphorylated by kinases at the cell membrane and are dephosphorylated in the cytoplasm. Let us first illustrate the case where this spatial separation generates a spatial gradient of a single phosphoprotein. For simplicity, we consider a steady-state situation[160,161] where the concentration of phosphoprotein P is governed by the reaction-diffusion equation of the form[162] $0 = D\nabla^2 P(x) - k_P P(x)$. k_P is the rate constant of dephosphorylation (usually well approximated as first-order[163]), and the spatial coordinate is rescaled such that $x = 0$ corresponds to the membrane, and $x = 1$ to the surface of the nucleus. Solving this equation with a no-flux boundary at the surface of the nucleus gives the concentration profile that decays with the distance from the membrane approximately exponentially, $P(x) \propto \exp(-x/L_{grad})$, where $L_{grad} = \sqrt{D_P/k_P}$ is the characteristic decay length. For the typical values[163] $D_P \approx 1 \times 10^{-7}\,\mathrm{cm^2\,s^{-1}}$ and $k_p \approx 1\,\mathrm{s^{-1}}$, the distance over which the concentration P decreases by roughly an order of magnitude is about 7 µm, which is commensurate with the radius of a typical eukaryotic cell. An important consequence is that the phosphoprotein signal[163] reaching the nucleus is predicted to be markedly attenuated, thereby reducing the efficiency of the cell's response to the signal or even eliminating such a response altogether in larger cells (for example, the signal reaching the nucleus in *Xenopus oocytes* of size ca. 1 mm would be attenuated by the factor of 10^{-140}!).

Cells have developed several RD strategies to overcome such signal attenuation. One strategy is to change the shape of the cell. Unlike prokaryotes, which have fairly constant and non-deformable shapes (for example, spherical *Streptococcus* or rod-shaped *E. coli*), eukaryotes can flatten, spread out, and extend thin protrusions during substrate adhesion and cell migration. In a migrating cell, these events define a thinner leading edge and a thicker trailing edge; not surprisingly, phosphorylation-based signaling occurs mostly near the leading edge, where the distance the signal needs to travel to the nucleus is shorter than that through the trailing edge[74] (Figure 9).

Another possibility is signaling through "cascades" involving multiple phosphoproteins arranged in units relaying the signal in a domino-like fashion. For example, in the mitogen-activated protein kinase (MAPK) signaling cascade illustrated in Figure 10b, MAPKKK (a kinase of kinase MAPKK) becomes phosphorylated, and thus activated by upstream receptor kinase at the cell membrane. This phosphorylated MAPKKK (MAPKKK-P) subsequently phos-
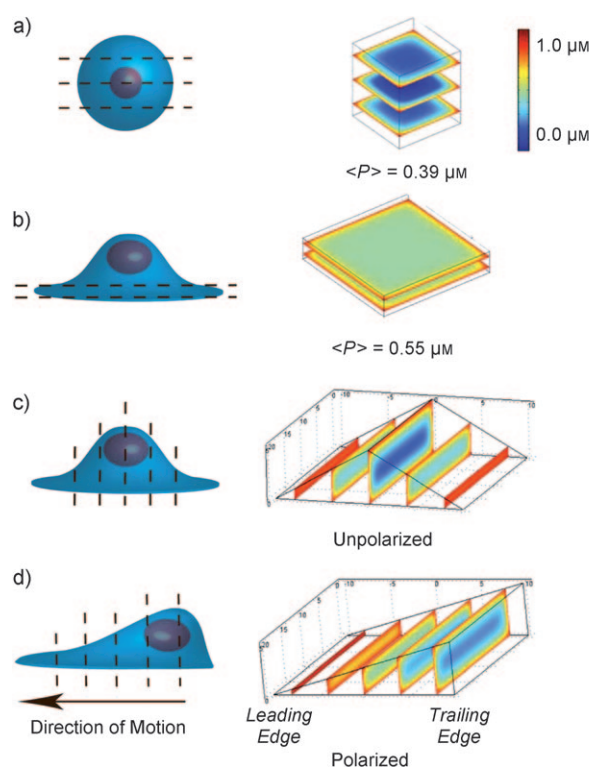

Figure 9. Changes in cell shape as a strategy of regulating the efficiency of phosophoprotein-based signaling. The graphs in a)–d) give a schematic view of the cell shapes and the corresponding phosphorylation profiles (that is, the concentrations of the phosphoprotein P) along the dashed cross-sections. The profiles are calculated on the basis of the single-phosphoprotein model discussed in the main text. In all cases, the volume of the cells is kept constant at ca. 1000 µm³ and the concentration at the cell membrane is set to 1 µM. A comparison of the spherical cell in (a) and adherent cells in (b) demonstrates that cell flattening (as occurs during attachment of the cell to a solid surface) leads to higher levels of phosphorylation. The average concentrations of P within the cell are 0.39 µM for the spherical cell and 0.55 µM for a flattened cell. In c) and d) unpolarized and polarized cells, respectively, are compared. In (c), the phosphorylation profile is symmetric with respect to the cell's axis of symmetry. d) When, however, the cell is polarized, the leading edge is thinner and thus more phosphorylated than the trailing edge. Images to the right of the cell schemes are reproduced with permission from Meyers et al.[74]
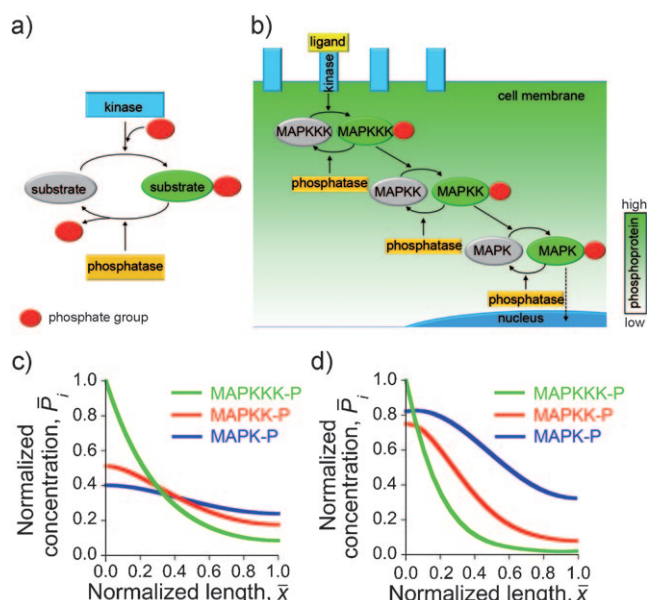
Figure 10. Signaling pathways in eukaryotes. a) A motif commonly found in signaling pathways. The signaling protein (substrate) cycles between two forms—phosphorylated (active; the red circle denotes a phosphate group) and dephosphorylated (inactive) in a process mediated by two enzymes of "opposing" activities. b) Scheme of the mitogen-activated protein (MAP) kinase cascade. The receptor kinase becomes activated by binding to an extracellular ligand. The activated receptor kinase phosphorylates and thus passes the activation signal to MAPKKK. Phosphorylation activates MAPKKK, which is now able to catalyze the phosphorylation and activation of its downstream target, MAPKK. This process continues "down" the cascade until the signal reaches the nucleus where the cellular response is triggered. The active forms of MAP kinase enzymes (MAPKKK-P, MAPKK-P, MAPK-P) are dephosphorylated by phosphatases homogenously dispersed in the cytoplasm. Spatial separation of the receptor kinase (cell membrane) and phosphatase (cytoplasm) leads to the formation of the phosphoprotein gradient directed from the cell membrane towards cell nucleus. c,d) Steady-state concentration profiles of the phosphorylated kinases. c) The concentration profiles of a simplified model discussed in the main text. Near the nucleus, at $x=1$, the concentration of MAPK-P is about three times that of MAPKKK-P. d) A more sophisticated theoretical treatment (see Ref. [164]) predicts the concentration of MAPK-P at the nucleus surface to be about 20 times higher than that of MAPKKK-P.

phorylates MAPKK (a kinase of MAPK) in the cytoplasm. Similarly, the phosphorylated MAPKK (MAPKK-P) activates MAPK (MAP kinase) before MAPK-P activates its downstream targets, triggering a specific biological response (that is, expression of specific genes).[75]

To see how such cascading facilitates signal transduction, let us again consider a steady-state model, but this time accounting for several phosphorylated kinases, each obeying a reaction-diffusion equation of the form[164] $0 = D\nabla^2 P_i(x) + R_{kin}(x) - R_{pho}(x)$, where x, as before, denotes a rescaled spatial coordinate, $P_i(x)$ stands for the normalized concentration of the phosphorylated kinase for the i-th species "down" the cascade (namely, P_1 is the concentration of MAPKKK-P, P_2 of MAPKK-P, and P_3 of MAPK-P), R_{kin} is the phosphorylation rate of the respective unphosphorylated kinase, and R_{pho} is the dephosphorylation rate arising from the reaction with phos-

phatase. With reference to Figure 10b and writing out the expressions for the reaction rates explicitly, one obtains the system of steady-state RD equations [Eq (10)].

$$D\nabla^2 P_1(x) - k_1 P_1(x) = 0$$
$$D\nabla^2 P_2(x) + k_2 P_1(x) - k_3 P_2(x) = 0 \qquad (10)$$
$$D\nabla^2 P_3(x) + k_4 P_2(x) - k_5 P_3(x) = 0$$

Here, the terms involving rate constants k_1, k_3, and k_5 describe the dephosphorylation of the respective species P_1, P_2, and P_3 in the cytoplasm, while the terms involving k_2 and k_4 refer to the generation of P_2 and P_3 by their upstream kinases P_1 and P_2, respectively. The species P_1 is generated at the cell membrane and this process is accounted for by a fixed boundary condition $P_1(x=0) = $ constant; the other boundary conditions are no-flux of any species at the surface of the nucleus, $\partial P_i(x)/\partial x \mid_{x=1} = 0$.

When solved numerically, the solutions of the "cascade" model can be plotted as a function of the rescaled distance. The comparison to make here is between the concentration of MAPK-P reaching the nucleus at $x=1$ and the concentration of MAPKKK-P (which, in the one-protein model described earlier, would be the only phosphoprotein present) at the same location. Figure 10c shows that the ratio of these concentrations is close to three, thus indicating that the presence of the "cascade" effectively amplifies the signal reaching the nucleus. The amplification effect is even more pronounced—with concentration ratios at the nucleus as high as 20—in models in which the kinetics of phosphorylation/ dephosphorylation is treated more accurately (Figure 10d and Ref. [164]). Even with these improvements, however, the RD cascades (or even active-transport mechanisms based on microtubular transport) are still insufficient to explain signaling in very large cells such as 1 mm *Xenopus oocytes*. While some RD models have attempted to resolve this issue by introducing feedbacks from downstream to upstream kinases,[165] the controversy is far from resolved and remains an object of active research.

Another intriguing example of how RD accelerates and amplifies signaling—this time over the two-dimensional manifold of a cell membrane—is the so-called lateral phosphorylation propagation (LPP).[166] In this process, some epidermal growth factor receptors (EGFR) residing in the membrane are locally stimulated by specific ligands from the environment. After ligand binding, the conformation of EGFR changes so that it can now bind ATP; this, in turn, increases the intrinsic kinase activity of the EGFR and allows it to phosphorylate other receptors.[167] For this "lateral" phosphorylation to happen, EGFRs not yet activated must diffuse towards and interact with the activated EGFR center (Figure 11, left). However, since the activated centers are sparse, the inactive EGFRs would have to diffuse over relatively large distances—on average, $L = 20$ μm.[166] For a diffusion coefficient of EGFR within the membrane of $D \approx 3 \times 10^{-10}$ cm^2 s^{-1},[168] the activation time (time required to activate receptors on the entire cell surface) would then be on the order of $\tau \sim L^2/D \approx 200$ min. In reality, experiments with MCF7 breast adenocarcinoma cells demonstrate that the
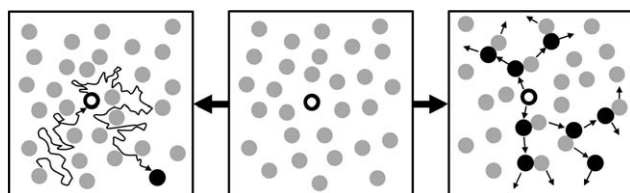
Figure 11. Lateral phosphorylation propagation (LPP): Comparison between the diffusion-based (left panel) and reaction-diffusion-based (right panel) models. Gray circles: inactive receptors; open circles: receptor activated by an extracellular ligand; black solid circles: receptors activated by the active receptor(s). The initial condition (middle) shows one locally activated receptor. In the purely diffusive mechanism, each inactive receptor has to diffuse long distances—first, to the active center to become activated, and then away from it to make room for other receptors. This is a very inefficient and slow (several hours) mode of receptor activation. In contrast, in the reaction-diffusion scenario, the activated receptors can pass their activated status to their neighbors, which need to diffuse only short distances to the nearest activated sites. This RD process results in rapid (seconds) activation of many receptors.

Figure 12. a) Time-lapse confocal images of a calcium wave in starfish embryos. The embryos are fertilized in the left-hand portion of the cell (indicated by white triangular arrows), and the wave propagates towards the right of the cell. The time for the wave to propagate throughout the entire cell is approximately 45 s. Reproduced with permission from Stricker.[174] b) Computer simulation of the Ca^{2+} wave propagation through a circular domain assuming a hypothetical, purely diffusive mechanism. The wave is initiated on the left and propagates towards the right. The front is much more diffuse compared to the experimental images in (a), and the time of propagation is significantly longer—here, about 50 h compared to less than a minute in experiments. The simulations were performed with a constant Ca^{2+} concentration maintained at the injection site, no-flux boundary conditions around the rest of the cell's perimeter, and with the diffusion constant of calcium $D = 6 \times 10^{-8}\ cm^2 s^{-1}$.

activation process happens much faster, within about 1 minute.[168] To explain this discrepancy it has been suggested[166] that instead of all the inactivated EGFR diffusing to the activation centers, the receptors need to diffuse only locally to the nearest phosphorylated receptor, and become phosphorylated therein. Once phosphorylated, this newly activated center can then pass the phosphorylated state to its neighbors and the "cascading" effect continues (Figure 11, right). To see whether this scenario would indeed accelerate the activation process over a domain of size L, let us consider the familiar scaling arguments. Let δL be the average distance between two receptors (not only the activated ones) and $N = L/\delta L$ be the number of RD activation events that need to take place before all receptors become activated. The total activation time is then $\tau \sim N(\delta L)^2/D = L\delta L/D$.[166] For example, in human fibroblasts, the total number of receptors on the cell surface is $n_R \approx 100\,000$,[169] the cell radius is $r \approx 10\ \mu m$,[170] and the area per receptor is $\pi r^2/n_R = 0.003\ \mu m^2$. This value corresponds to an average distance between receptors of $\delta L \approx 60\ nm$, and an activation time of only about 40 s, which is close to the experimentally observed values.

4.1.2. Calcium Waves

Intracellular free calcium (Ca^{2+}) is a key secondary messenger involved in eukaryotic cell signaling that underlies fertilization, cell growth, transformation, secretion, smooth muscle contraction, sensory perception, and neuronal signaling.[171–173] Calcium signaling typically manifests itself in the form of Ca^{2+} waves which sweep across the cells (Figure 12 a). In egg cells, such waves are triggered by a sudden local rise in the cytosolic Ca^{2+} concentration upon fertilization, and their propagation across the cell marks the onset of embryonic development.[75, 174] Although Ca^{2+} waves may appear similar to simple diffusive fronts, neither the speed of their propagation nor the sharpness of the front are characteristic of pure diffusion. For example, experiments have shown that the average velocity of the calcium wave in *Xenopus* eggs is
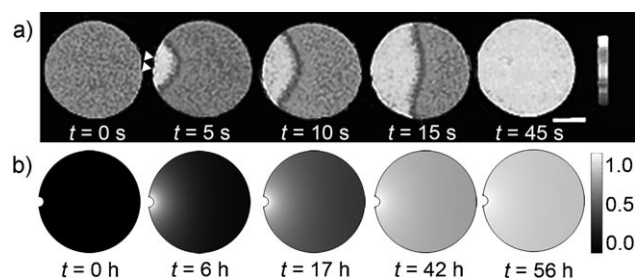
approximately 10 $\mu m\,s^{-1}$, and it takes approximately 1 minute to fill up a 1 mm cell with Ca^{2+}.[175] In sharp contrast, computer simulations that assume simple diffusion over the same domain (with diffusion coefficient $D \approx 6 \times 10^{-8}\ cm^2 s^{-1}$, typical of Ca^{2+} in cells[176]) predict "filling" times of about 50 h (Figure 12 b). In addition, diffusion alone is unable to account for the more complex modes of Ca^{2+} propagation observed in some cases (for example, circular or spiral patterns[171, 177] that resemble classical Belousov–Zhabotinski (BZ) waves;[178] see Figure 13 f).

To explain the mechanism of wave propagation, we first note that the concentration of Ca^{2+} in the cytosol is normally kept low (ca. 20–100 nM[173]) by binding to cytoplasmic Ca^{2+}-binding proteins to avoid the cytotoxic effects of calcium.[179] Larger amounts of calcium are stored intracellularly in endoplasmic or sarcoplasmic reticula (ER/SR) "connected" to the cytosol through Ca^{2+} channels and pumps (Figure 13 a). When calcium is "injected" into the cell from an external source, the ER/SR channels are put into action by a process known as calcium-induced calcium release (CICR). In this process, each ER/SR releases its own Ca^{2+} when exposed to Ca^{2+}, which, in turn, influences neighboring ER/SRs and ultimately enables rapid propagation of Ca^{2+} waves. The key elements of the CICR are 1) the autocatalytic release of Ca^{2+} from the reticula, and 2) the nonlinear coupling between the local calcium concentration and the activity of calcium channels/pumps. These elements can be described by the RD Equations (11) and (12).[180, 181]

$$\frac{\partial c}{\partial t} = D\nabla^2 c + J_{rel}(c, n) - J_{pump}(c) \tag{11}$$

$$\frac{\partial n(c)}{\partial t} = (n_\infty - n(c))/\tau_n \tag{12}$$

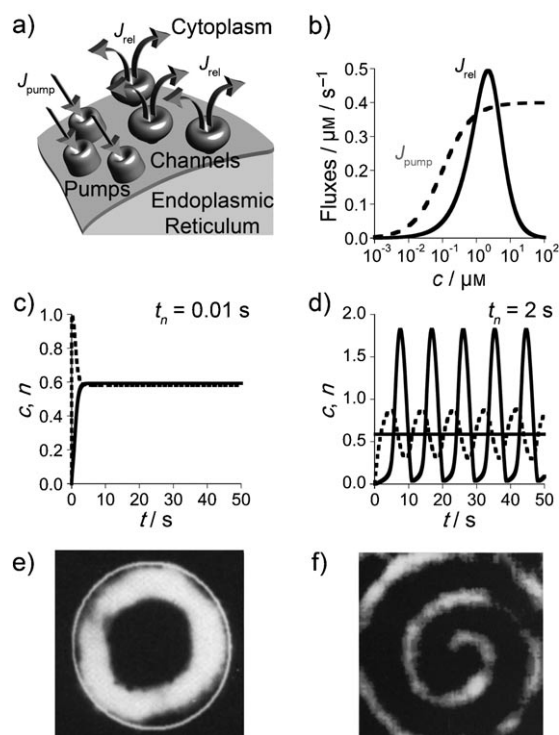Here, c is the concentration of Ca^{2+} at a given spatial

Figure 13. Calcium oscillations and waves. a) Fragment of the endoplasmic reticulum which can store and release Ca^{2+} ions. The release (characterized by J_{rel}) is mediated by calcium channels. Calcium pumping into the ER/SR (J_{pump}) occurs through calcium pumps. b) Qualitative dependence of J_{rel} and J_{pump} on the concentration of cytosolic calcium, c. c,d) Calculated calcium concentrations c (solid curves) and the number of channels open n (dashed curves) plotted as a function of time t for two cases: c) channels responding instantaneously to the changes in c (that is, τ_n is small, here 0.01 s), and d) channels responding with a time lag (that is, τ_n is large, here 2 s). In the former case, the system attains a steady state; in the latter case, the calcium concentration oscillates from below to above the steady-state levels. c is given in μM, and n is expressed as a fraction of the total number of channels. The horizontal line in (d) corresponds to the steady-state levels from (c). e) Target and f) spiral waves observed in *Xenopus Oocytes* after injecting the cells with Ca^{2+}.[177] Parts (e) and (f) are reproduced with permission from Lechleiter and Clapham.[177]

location and time, J_{rel} is the rate at which Ca^{2+} is released from the ER/SR into cytoplasm, and J_{pump} is the rate at which cytoplasmic Ca^{2+} is pumped back into the ER/SR. n is the fraction of Ca^{2+} channels opened for Ca^{2+} release, n_∞ is the steady-state value for n, and τ_n is a parameter that characterizes the rate of the channel's response to the changes in c: if τ_n is small, $\partial n/\partial t$ is large and the response is fast; if τ_n is large, $\partial n/\partial t$ is small and the response is slow.

While various functional forms of the fluxes J can be conceived, both experiments[182, 183] and models[180, 184] indicate that their key feature is the bell-shaped dependence of the release flux J_{rel} on the local calcium concentration (Figure 13b). In the low-concentration regime, the number of open channels n and the efflux of Ca^{2+} increases autocatalytically with increasing c. When, however, c increases further, the channels close and Ca^{2+} outflow from ER/SR decreases to avoid the toxicity of calcium.[179] Mathematically, these effects

translate into a coupling between Equations (11) and (12)—that is, c being dependent on n [through $J_{rel}(c,n)$ in Eq. (11)], with n being dependent on c [through $n(c)$ in Eq. (12)]. At the same time, the flux of calcium pumped back into the ER/SR (J_{pump}) depends only on c, with which it is usually assumed to increase monotonically in a sigmoidal fashion (Figure 13b[184]).

The formation of a calcium wave can then be described as follows. When a cell is stimulated with external Ca^{2+} (or with a hormone or a neurotransmitter "agonist" involved in the production of inositol 1,4,5-triphosphate (InsP₃) that helps open calcium channels[173]), Ca^{2+} is released autocatalytically from the ER/SR stores close to the stimulation site. As more and more Ca^{2+} is released, the channels start closing, while Ca^{2+} is also continually being pumped back into the ER/SR. At a certain critical concentration of Ca^{2+}, the rate of release (J_{rel}) balances that of back-pumping (J_{pump}) and a steady-state is reached. This state maintains a relatively high concentration level of Ca^{2+} compared to an unstimulated cell. Since the "extra" dose of Ca^{2+} released into the cytoplasm can also diffuse, it can trigger release from the neighboring ER/SR sites, where the efflux/influx process repeats. This "domino" effect continues in the form of a calcium wave that sweeps across the whole cell and ultimately leaves it "activated" in the high-calcium state.[179] This state can persist for up to tens of minutes, but ultimately, in the so-called recovery phase, decays as Ca^{2+} is pumped out of the cell, through the channels in the cell membrane.[172]

The first Ca^{2+} wave sweeping through the cell is important for many biological functions. For example, after fertilization, the wave of Ca^{2+} is thought to provide essential signals that enable normal development of the embryo.[174] In smooth muscle cells, Ca^{2+} waves cause the cells to relax or contract.[179] In particular, when small, localized pulses of Ca^{2+} are introduced near the plasma membrane of the muscle cell, this cell relaxes. If, however, the external stimulus is strong enough to initiate autocatalytic release of Ca^{2+} from ER/SR so that the Ca^{2+} wave propagates across the whole cell, the muscle cell contracts. In another example, Ca^{2+} waves regulate chloride (Cl⁻) secretion from exocrine pancreatic cells into the lumen of the intestine, where Cl⁻-rich pancreatic fluid neutralizes the gastric hydrochloric acid.[185] The concentration of Ca^{2+} rises selectively at the luminal pole of the cell in response to external stimulation. This opens a set of membrane channels through which Cl⁻ ions are secreted out of the cell. As the Ca^{2+} wave initiated at the luminal pole spreads across the cell toward the basolateral side, another set of channels becomes activated, thereby resulting in the uptake of Cl⁻ ions by the cell, which is important for maintaining the unidirectional secretion of chloride ions.[185]

The fascinating calcium RD story does not necessarily end with the passage of the first wave. Experiments[177] have shown that some regions in the cell are naturally excitable and, after the first calcium wave subsides, can continue to oscillate between high and low Ca^{2+} concentrations. Although the biological reasons why certain regions sustain oscillations while others do not are still being debated,[186] the mechanism of the oscillations can be explained by the familiar RD Equations (11) and (12) (with the diffusive term neglected for

oscillations occurring in one location). The key parameter here is the channel response time τ_n.

When τ_n is small, the channels respond to the changes in the Ca^{2+} concentration (by opening or closing) almost instantaneously. The dynamics of the system is then governed by the ratio of the J_{rel} and J_{pump} fluxes and, as we have seen earlier, leads rapidly to a steady-state where there is no further increase or decrease in the Ca^{2+} levels (Figure 13 c). This behavior changes dramatically, however, when τ_n is large. Under these conditions, the channels respond to concentration changes with a pronounced time lag. Initially, at low levels of Ca^{2+}, more Ca^{2+} is released from ER/SR by the "autocatalytic" CICR mechanism. After reaching a sufficiently high Ca^{2+} concentration, the "outflow" channels start to close, but the closure is slow and cannot prevent the cytosolic calcium concentration from reaching values as high as 1.8 μM, that is, significantly higher than for the steady-state that would be expected with an immediate channel response. Only when the cytosol is flooded with extra calcium, are the "outflow" channels finally closed and the cell relieves its unnatural high-calcium state by pumping Ca^{2+} back into the ER/SR. While this continues, the "outflow" channels start opening but, again, they do so slowly, with a time lag. As a result, the levels of Ca^{2+} in the ER/SR become unnaturally high, whereas those in the cytosol, become unnaturally low (down to ca. 0.04 μM). When the channels finally reopen, the rapid outflow begins and the outflow/inflow cycle repeats. All in all, the lags in the channel response enable the system to increase the Ca^{2+} levels rhythmically above and then below a putative steady-state, which is never attained (Figure 13 d).

Oscillations in the Ca^{2+} concentration are important in the regulation of nuclear signaling, that is, regulation of gene expression by transcription factors (TF).[187,188] Unlike in the case of constant but low Ca^{2+} concentrations, oscillations can periodically exceed the threshold concentration required for TF activation and can thus increase signaling efficiency.[187] In addition, the frequency of Ca^{2+} oscillations can control gene expression.[189] For example, studies of gene expression driven by three transcription factors in T lymphocytes demonstrated[187,188] that infrequent Ca^{2+} oscillations activate only one of these factors, whereas high-frequency oscillations recruit all three of them, thereby leading to frequency-specific expression of proinflammatory cytokine genes. In vitro experiments suggest that CaM kinase II (Ca^{2+}/calmodulin-dependent protein kinase II) plays a central role in these events by decoding the frequency of the oscillations into distinct degrees of kinase activity.[190] Finally, when local oscillations are coupled with diffusion, they can affect nearby ER/SR stores and give rise to multiple Ca^{2+} waves that propagate throughout the cell as target patterns or spirals[171,177] (Figure 13 e,f). Although the role of these complex spatiotemporal structures is still not understood, it has been proposed that the information encoded in their amplitude, frequency, and mode of propagation influences intracellular signaling.[171,177]

Directing a reader interested in more examples of RD-based signaling to Refs. [165,191], and to Refs. [192,193] for the discussion of calcium-related NAD(P)H waves, we now turn our attention to reaction-diffusion processes involving larger, cytoskeletal structures. Recall from Section 3.2 an intricate mechanism in which concentration oscillations of Min proteins mediated division of prokaryotic cells. In the next section, we will see how eukaryotes achieve the same result with a very different mechanism[194] involving coupling of RD to cytoskeletal fibers called microtubules.

4.2. Self-Organization of the Mitotic Spindle Driven by Chromosome-Generated Ran-GTP-Dependent Gradients

Microtubules (MTs) are hollow tubes built of 13 protofilaments comprised of α- and β-tubulin heterodimers. In eukaryotic interphase (nondividing) cells, MTs are often organized in a radial array, emanating from the centrosome located roughly at the center of the cell. MT minus ends are capped and anchored at the centrosome, while plus ends stochastically alternate between phases of growth and shrinkage, thus exploring the cytoplasm. In preparation for cell division, centrosomes localized in the cytoplasm duplicate and nucleate two radial arrays of MTs that are shorter and more dynamic than those in the interphase array. Once the nuclear envelope breaks down, the MT plus ends of these two arrays gain access to the chromosomes. Within minutes, microtubules and their associated proteins (including motor proteins) assemble into bipolar mitotic spindle, which distributes duplicated chromosomes to the two daughter cells with astounding precision. As the spindle assembles, the MT plus ends are targeted towards chromosomes and when captured by kinetochores (protein complexes at the middle of each chromosome), MTs attach in a stable manner and generate forces that pull the chromosomes of each pair towards the two opposing cell poles.[195]

Although the targeting and attachment of MTs to chromosomes was originally thought to be a random "search-and-capture" process,[196] subsequent computational analysis showed that it would be far too inefficient to explain how MTs get connected to all (46 pairs in human cells) kinetochores in the short time (ca. 30 min) needed to complete mitosis. Instead, it was shown that search-and-capture biased toward the chromosomes could account for the experimentally observed rates of MT capture.[197] In addition, experiments with acentrosomal eukaryotic cell systems (for example, many oocytes, higher plant cells, and also animal cells with destroyed centrosomes) where mitotic spindle can self-organize in the absence of centrosomes indicated that some guiding signal for the assembly of the spindle comes from the chromosomes[198–201]—this signal and also the key conserved player of mitotic spindle assembly is Ran, a small GTPase of the Ras superfamily.[202] Relevant to our discussion is that it is reaction-diffusion that generates a series of Ran-GTP-dependent gradients around mitotic chromosomes and that these gradients orchestrate the assembly of mitotic spindle by providing positional cues for MT nucleation, centrosomal MT stabilization, and eventual asymmetric or biased MT growth towards chromosomes.[162,203,204]

The complex sequence of events that leads to the formation of these gradients can be described as follows (Figure 14 a). The concentration of Ran-GTP is high near the
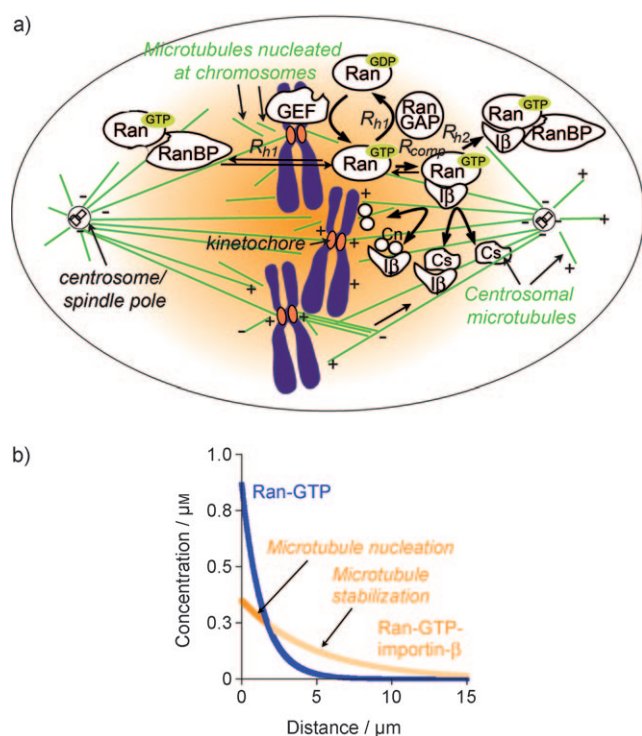
Figure 14. Gradient of Ran-GTP-importin-β complexes and the formation of mitotic spindle. a) Scheme of an assembling mitotic spindle. MTs (green, long tubules) nucleated at the centrosomes at each pole of a dividing cell grow asymmetrically towards the chromosomes (blue) at the center of the cell. In addition, MTs are also nucleated at the chromosomes (short, green tubules); these MTs are also incorporated into the final bipolar spindle. Ran-GTP generated at the chromosomes diffuses through the cytoplasm and forms various protein complexes (see main text for a detailed discussion of the interactions shown). Complexation with cytoplasmic importin-β gives rise to a steep Ran-GTP gradient and a further-reaching gradient of Ran-GTP-importin-β (orange cloud). b) Plot of the gradients as a function of distance (where $x = 0$ is the location of chromosomes). The gradients provide spatial cues for MT nucleation at the chromosomes and for asymmetric centrosomal MT growth. The Ran-GTP-importin-β gradient has different short-range and long-range effects through the release of two types of NLS-containing importin-β cargo proteins. The release of the first of these cargos (Cn) enables MT nucleation close to the chromosomes; the release of the second cargo (Cs) stabilizes MT growth further away and thus directs centrosomal MT growth towards the chromosomes.

chromosomes, while that of Ran-GDP is high in the cytoplasm. This difference is due to the spatial separation of proteins that interconvert the two Ran forms. The Ran guanine exchange factor (GEF) localized exclusively at the mitotic chromosomes converts Ran-GDP into Ran-GTP. On the other hand, as Ran-GTP diffuses away from the chromosomes, it is hydrolyzed to Ran-GDP either directly by cytoplasmic Ran-GTPase activating protein (RanGAP) or through interaction with RanBP1 (Ran-binding protein), thereby resulting in a steep gradient of free Ran-GTP around the chromosomes. Ran-GTP that is not hydrolyzed can bind to proteins of the importin-β family and form very stable Ran-GTP-importin-β complexes. This complexation prevents Ran-GTP hydrolysis,[205] and allows the Ran-GTP-importin-β

complex to diffuse far away from the chromosomes before being converted back into Ran-GDP by cytoplasmic RanGAP. Overall, the gradient of Ran-GTP-importin-β extends further into the cell than the steep gradient of uncomplexed Ran-GTP.[203]

The key features of gradient formation and gradient extension are captured by a relatively simple but instructive RD model [Eqs (13) and (14); for a more detailed treatment, see Ref. [203]].

$$\frac{\partial Ran}{\partial t} = D_{Ran}\nabla^2 Ran - R_{h1} - R_{comp} \tag{13}$$

$$\frac{\partial Ran\beta}{\partial t} = D_{Ran\beta}\nabla^2 Ran\beta - R_{h2} + R_{comp} \tag{14}$$

Here *Ran* stands for the concentration of Ran-GTP, *Ranβ* for the Ran-GTP-importin-β complex in the cytoplasm; R_{h1} is the rate of Ran-GTP hydrolysis or depletion by other mechanisms, R_{h2} is the rate of Ran-GTP-importin-β consumption into other complexes and subsequent hydrolysis, and R_{comp} is the rate of Ran-GTP complexation with importin-β (Figure 14a). The key feature of the model is the fact that $R_{h1} \gg R_{h2}$. In the absence of complexation, the R_{h1} term rapidly depletes the Ran-GTP and makes its gradient steep and short-ranged. However, R_{comp} converts Ran-GTP into a more stable complex, which can diffuse further before being depleted by the slow R_{h2} reaction. When implemented with physically reasonable parameters, this simple model predicts gradient ranges close to those observed experimentally in mitotic frog egg extracts[203] or in intact mitotic cells.[206,207]

The formation of a long-range Ran-GTP-importin-β gradient is crucial for the assembly of mitotic spindle. This is because 1) importin-β binds to and transports several NLS-containing proteins (NLS = nuclear localization signal) that regulate MT dynamics and polymerization[208–210] and 2) complexation of Ran-GTP to importin-β releases these regulators.[209,210] Two distinct types of MT regulators—nucleators and stabilizers—are released at different locations to enable the short- and the long-range effects of chromatin on microtubule dynamics. The release of MT nucleators requires high concentrations of Ran-GTP-importin-β, and thus nucleation of new MTs occurs near the chromosomes. On the other hand, the release of MT stabilizers can take place at lower concentrations of Ran-GTP-importin-β, and therefore it can occur closer to the centrosomes (Figure 14b).[203]

Nucleation and the stabilization are both important for the assembly of the mitotic spindle. The plus ends of the MTs nucleated near the chromosomes localize onto the kinetochores. As these plus ends continue to polymerize, the minus ends are pushed "backwards" into the cytoplasm. These MTs bundle up and continue growing until their minus ends are captured and transported by a motor-protein-dependent mechanism along the centrosomal MTs toward the spindle pole.[211,212] Concurrently, the MTs emanating from the two centrosomes dynamically explore[213] the cytoplasm in search of the chromosomes' kinetochores. In this task, they are guided by RD-generated gradients[203] of signaling molecules (such as Ran-GTP described here, but also see Refs. [206] and [162]). These gradients effectively bias the growth of centro-

somal MTs toward chromosomes to ensure that all the chromosomes are attached to the spindle poles through multiple microtubules (ca. 15–30 MTs). Colloquially put, this two-way growth mechanism connects kinetochores to the centrosomes and the centrosomes to the kinetochores. Once bipolar MT attachment is achieved, the cell is ready for the next stage of mitosis—that is, for the partitioning of its genetic material.[214]

4.3. Eukaryotic Cell Motility

Having started the Review of RD in prokaryotes with the discussion of bacterial chemotaxis (Section 3.1), we will conclude our journey through the world of cellular RD with the analysis of a much more complex mechanism of self-propulsion and sensing in eukaryotes. Eukaryotic cell motility involves various cytoskeletal components that control cell shape, attachment to the environment, cell polarization status, protrusion of the cell's front, and retraction of its rear. The overall outcome of these subprocesses is the ability of the cell to move directionally, which is crucial during development,[215] in tissue repair and regeneration,[216] neural plasticity,[217] immune surveillance,[218] and also in pathological conditions such as cancer metastasis.[219,220] Relevant to our discussion is that reaction diffusion is important for coordinating the cell's motility machinery both in space and in time.

4.3.1. Pushing Forward: Actin

Globular actin (G-actin) is one of the most abundant and evolutionary conserved proteins and has the unique ability to polymerize into 3–7 μm long filaments[221] (filamentous actin, F-actin). F-actin is intrinsically polarized in the sense that actin monomers with bound ATP nucleotides (ATP-G-actin) are added to the (+) end (so-called "barbed" end) of the filament while the other, (−) end ("pointed" end) undergoes hydrolysis by the conversion of ATP to ADP and disassembly of actin monomers. In vitro experiments[222] with actin/ATP extracts indicate that these dynamic processes are of reaction-diffusion type[222] and give rise to the so-called treadmilling of actin filaments[222–224] in which the "barbed" end continues to grow at the expense of the shrinking "pointed" end. In migrating cells, actin filaments form at the leading edge of the cell, where they organize into a dense, branched network with the "barbed" ends oriented towards the cell membrane and the "pointed" ends directed toward the cell interior/rear. As the entire network treadmills[225] (Figure 15), it effectively "pushes" the cell membrane forward and allows it to form exploratory protrusions. These dynamic processes are essential for cell motility.

The consequence of network treadmilling is that since G-actin consumption is localized predominantly at the leading edge of the cell[226] while filament disassembly takes place in the interior/rear of the cell, a transportation mechanism must exist to recycle G-actin to the cell front to sustain polymerization and maintain directional cell migration.[227,228] Several RD models[227–229] that estimate the key parameters of the actin network turnover indicate that diffusion plays an
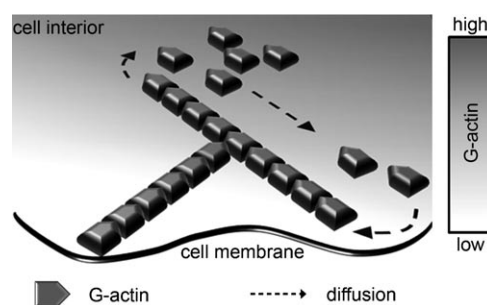

Figure 15. The actin treadmilling. Actin filaments form at the leading edge of a migrating cell, where they organize into a branched network, with their fast-growing "barbed end" facing the cell membrane and the slow-growing "pointed end" facing the cell interior. This intrinsic polarization of the actin filaments underlies the RD-based actin network "treadmill", in which the total length of F-actin remains approximately constant, but G-actin continuously polymerizes/extends at the barbed end while depolymerizing/shrinking at the pointed end (after debranching, see Ref. [225]). G-actin released from the pointed end of the filament diffuses down the concentration gradient towards the cell front where it reacts with the barbed end to become incorporated into the growing filament.

important role in G-actin transport. For example, for a treadmilling filament of average length $L = 5$ μm,[221,230] and for a diffusion coefficient of G-actin $D \approx 5 \times 10^{-8}$ cm^{2}s^{-1},[231] the characteristic diffusive time is on the order $\tau_D \sim L^2/D = 5$ s. On the other hand, the rate of consumption of actin monomers at the leading edge has been estimated[228] to be $k = 3$ s^{-1}, which gives $\tau_R \sim 1/k \approx 0.3$ s,[232] which is significantly smaller but not negligible compared to τ_D. This finding suggests that both the (slower) diffusion and the (faster) reaction components should be taken into account when modeling the treadmilling process. Although other estimates have also been proposed and the debate on the fundamentals of the treadmilling mechanism is still far from being resolved (see, for example, Ref. [233] for a discussion of pressure-driven transport), let us now examine the consequences of this phenomenon at the level of an entire cell.

One fascinating example here is the reaction-diffusion model developed by Mogilner and Edelstein-Keshet,[229] which accounts not only for the dynamics of the actin cytoskeleton, but also reproduces the resulting cell motion. While the details of this model are somewhat involved and beyond the scope of the present Review, the RD equations for the $N = 4$ G-actin species involved (see Ref. [229] for details) are of the general form of Equation (15).

$$\partial c_i / \partial t = -V \, \partial c_i / \partial x + D \, \partial^2 c_i / \partial x^2 + R(c_1, \dots c_N) \qquad (15)$$

Here, i is the index numbering these $N = 4$ species, and the reaction term accounts for the polymerization/depolymerization of various G-actins. The qualitative difference between this and "traditional" RD equations we have seen so far is in the "convective" term $V \partial c_i / \partial x$, which accounts for the fact that the frame of reference (in this case the cell) is moving with velocity V (Figure 16 a). In this way, the equations are effectively being solved in a moving frame of reference. The key question is then to relate the macromolecular-level events
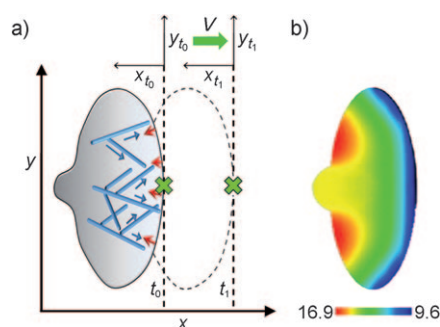
Figure 16. RD in a frame of reference of a moving cell. a) A motile cell (here, a keratocyte) has a polarized shape with a broad protrusion at the leading edge. Actin filaments polymerizing in a branching network (blue) push against the membrane, which offers elastic resistance (red arrows). The net motion of the cell depends on the balance between the two effects. RD equations describing intracellular RD processes are solved in the frame of the reference of the moving cell (cell velocity V). The key term, $\partial c_i / \partial x$, ensures that concentration gradients "move along" with the entire cell. The gray background represents the gradient of G-actin in the cell. b) A top-down view of a motile cell. The colors correspond to the concentration of G-actin calculated according to the model of Mogilner and co-workers[228] (less G-actin and more filamentous actin at the leading edge of the cell). A movie of the moving cell can be found at http://www.math.ucdavis.edu/~mogilner/CompKerat1.mpg.

of actin dynamics with the macroscopic motion of the cell. This is done by observing that while the polymerizing barbed ends of actin filaments push the membrane forward, the membrane offers some elastic resistance, and the net motion of the cell is determined by the balance between these two tendencies. The RD model gives the concentration of the barbed ends at the cell's membrane ($c_{x=0}$), and the expressions for the resistance F of the membrane (per unit length) have been developed independently[234–238]—hence, the velocity of the cell can be written in an analytical form $V = V(c_{x=0}, F)$. After these preparatory steps, the equations are solved numerically to reproduce cell motion and to derive several realistic parameters that describe this process. For example, the model predicts that the protrusion velocity V in rapidly moving cells is on the order of hundreds of $nm\,s^{-1}$, in agreement with experimental data. Furthermore, the model suggests that the optimal density of the barbed ends is roughly proportional to the membrane resistance. For experimentally estimated values of the resistance of $F = 50$–500 pN/μm, the theory predicts the optimal density of the barbed ends to be 25–250 per μm; the experimental value[239] is 240. This result has some intuitive basis: when there are too few barbed ends per unit length of the membrane, there is insufficient force to push the membrane; when, however, there are too many barbed ends, the pool of monomeric G-actin is depleted, so that there are too few monomers per filament available for the elongation of actin filaments and for "pushing" the cell forward. These and other accurate predictions of the model are, at least to us, quite a remarkable feat of RD modeling.

4.3.2. *Exploring the Surroundings: Filopodia and Membrane Ruffles*

The broad lamellipodium at the front of the cell not only pushes forward, but also supports membrane ruffles and spike-like protrusions (called filopodia[75]) through which the cell explores and senses the external environment. The basic machinery for lamellipodial and filopodial protrusions is provided by the dynamic network of actin filaments discussed in the previous section. For a cell to advance, however, the actin "push forward" is not enough and the newly extended protrusions must form stable attachments (adhesion sites[75]) to the surroundings. If these attachments are not formed, lamellipodial actin keeps polymerizing until it collapses backwards, and "unproductive" wavelike membrane ruffles form instead.[240, 241]

Remarkably, the formation of the various structures at the cell's leading edge can be explained by a single RD model[242–244] which combines membrane dynamics, diffusion of membrane lipids or proteins that activate actin polymerization (referred to as "activators"), and protrusive forces resulting from G-actin polymerization at the leading edge.[243] Whether the leading edge of a migrating cell develops membrane ruffles or protrudes filopodia depends on the local curvature of the membrane, which is itself related to the local concentration of the activators. This coupling between concentration and geometric curvature requires additional terms to be included in the RD equation for the system. One astute choice is Equation (16).

$$\frac{\partial c}{\partial t} = D\nabla^2 c - H\nabla^4 h + \eta \tag{16}$$

Here, c is the concentration of activators in the membrane, D is their diffusion coefficient, h measures the normal displacement of the membrane from a flat reference plane (this displacement is governed by an integral-differential equation of membrane dynamics, see Ref. [243] for details), and η accounts for the motion of the activators arising from the random/stochastic events in the cell. The meaning of the key, fourth-order derivative term of h can be grasped by noting that the membrane's curvature κ can be approximated as $\kappa \approx \nabla^2 h$. For the activator proteins to aggregate in the regions of maximal/minimal curvature, these proteins have to migrate along the gradients of curvature. Mathematically, this means that the flux of these proteins $\vec{j}$ is proportional to $\nabla^3 h$. Together with the usual diffusive flux $\vec{j}$ we then have $\vec{j} = -D\nabla c + H\nabla^3 h$ and, from the conservation of mass, $\partial c / \partial t + \nabla \vec{j} = 0$ (see Section 2), we obtain $\partial c / \partial t = D\nabla^2 c - H\nabla^4 h$.

The elegance of this formulation is that the dynamics of the system is effectively determined by the sign of only one parameter H, which reflects the relationship between the membrane curvature and the concentration of the activator proteins. When $H > 0$, the activators tend to aggregate at locations of maximum curvature (Figure 17 a). With a higher concentration of activators at these loci, more actin polymerization occurs there, which, in turn, generates more protrusive forces that act on the membrane. These forces cause further
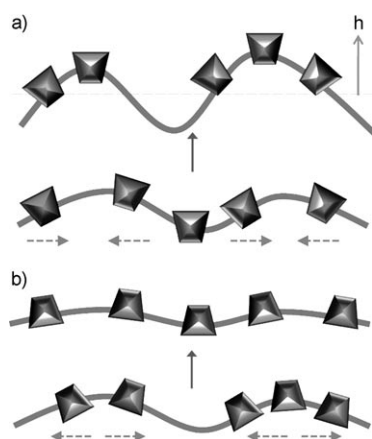
4188   www.angewandte.org

© 2010 Wiley-VCH Verlag GmbH & Co. KGaA, Weinheim

Angew. Chem. Int. Ed. **2010**, *49*, 4170–4198

Figure 17. The formation of filopodia and wavelike membrane ruffles depends on a subtle interplay between membrane curvature, diffusion of the activator proteins in the membrane, and the degree of actin polymerization. a) For $H>0$ (see text for details), activators tend to aggregate at the locations of highest curvature. Therein, they promote the polymerization of actin and generate more protrusive forces on the membrane, effectively increasing the curvature and causing further accumulation of activators (positive feedback). b) For $H<0$, activators tend to aggregate at locations of minimum curvature. Whenever thermal/random fluctuations bend the membrane, the activators rapidly diffuse out of the curved regions, thereby limiting actin polymerization and causing the membrane to flatten (negative feedback). Dashed arrows indicate the direction of motion of the activator proteins.

Figure 18. Irreversible vsersus reversible cross-linking of actin filaments by fascin. a) Illustration of fascin diffusing into the filopodium where it binds/cross-links actin filaments irreversibly. According to this mechanism, fascin cannot be delivered to the tip of the filopodium as rapidly as the filopodium elongates. Consequently, the tip region remains un-cross-linked and is not mechanically sturdy. b) The net transport of fascin into the filopodium is faster for reversible fascin/actin binding. c) Plot of the percentages of cross-linked filaments c_C/c_{A0} for the scenarios of reversible ($k_{off}=0.12$ s^{-1}, gray curves) and irreversible ($k_{off}=0$ s^{-1}, black curves) binding. Dotted curves correspond to filopodia that are 3 μm long—in this case, cross-linking reaches the tip of the filopodium with either reversible or irreversible binding. When, however, the filopodium is longer (for example, 10 μm, solid curves), cross-linking extends to the tip only for the reversible binding (solid gray curve). Data used to create the plots are taken from Ref. [250].

increase in the curvature and, eventually, the formation of spike-like filopodial protrusions; in other words, the system exhibits positive feedback with the filopodia growing autocatalytically until their growth is restricted by membrane resistance.[245,246] Conversely, if $H<0$, the membrane activators tend to aggregate at the locations of minimal membrane curvature (Figure 17b). If thermal/random fluctuations bend the membrane at some places, the activators rapidly diffuse out of these curved regions, thereby limiting actin polymerization in these regions and causing the curvature to decrease. This is an example of negative feedback, where the system annihilates any disturbances of the membrane and tries to keep it flat. The continual tug-of-war between membrane deformation and flattening gives rise to membrane ruffles/waves rather than filopodial protrusions. It is important to note, however, that a cell membrane typically has regions with $H>0$ and with $H<0$, so there are filopodia in some locations and ruffles in the others. Where these regions are located is not completely understood, but experimental evidence suggests that Cdc42 proteins play the key role in the former case, and Rac proteins in the latter.[247,248]

For efficient exploration of the cell's surroundings the filopodia must be flexible and bendable, yet rigid enough to protrude many micrometers from the cell's surface. The latter cannot be achieved with filopodia containing individual/un-cross-linked actin filaments which bend and buckle easily under the stress of the cell membrane.[249] To increase rigidity, a protein called fascin cross-links the newly polymerized F-actin along the length of the filopodia into thicker and stiffer bundles.[249] For this cross-linking to proceed, fascin must be delivered to the tips of the filopodia from the cell body. One
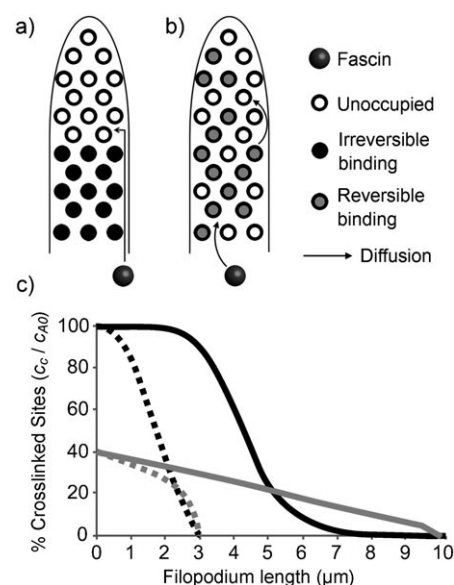
possibility is that fascin could be delivered by diffusion and, while migrating through the filopodia, undergo irreversible association with the un-cross-linked filaments until all the filopodial actin becomes bundled (Figure 18a).[250] However, it has been determined experimentally that the rate of filopodial growth (typically, 2–3 μm min^{-1}) is too rapid to be explained by the diffusion times involved [see Equations (17)–(19)].[250] To account for this discrepancy it has been suggested that migrating fascin binds to actin reversibly ($F+A\rightleftarrows C$), where F denotes free fascin, A stands for un-cross-linked actin filaments, and C denotes the filaments cross-linked with fascin. According to this mechanism, fascin diffusing from the interior of the cell shifts the local cross-linking equilibria within the filament and effectively "pushes" the fascin already present/bound therein towards the tip of the filopodium (Figure 18b). Qualitatively, this process is reminiscent of the domino-like RD we have seen before in, for example, lateral phosphorylation propagation (LPP, see Section 4.1.1). A familiar set of RD equations [Eqs. (17)–(19)] can describe this process.

$$\frac{\partial c_F}{\partial t} = D\frac{\partial^2 c_F}{\partial x^2} - k_{on}c_F c_A + k_{off}c_C \tag{17}$$

$$\frac{\partial c_A}{\partial t} = -k_{on}c_Fc_A + k_{off}c_C \tag{18}$$

$$\frac{\partial c_C}{\partial t} = k_{on}c_Fc_A - k_{off}c_C \tag{19}$$

Here, k_{on} and k_{off} represent the rate constants for the binding and unbinding of fascin to/from actin filaments, respectively; the filopodium is approximated as a long, 1D domain ($x = 0$ corresponds to the base and $x = L$, to the tip of the filopodium), and fascin F is the only diffusible species. Initially, there are only un-cross-linked actin filaments in the filopodia ($c_A(t{=}0) = c_{A0}$), but no cross-linked filaments or fascin ($c_C(t{=}0) = c_F(t{=}0) = 0$). The concentration of fascin is maintained at the base of the filopodium ($c_F(x{=}0,t{>}0) = c_{F0}$), but there is no flux of c_F at the tip ($\partial c_F(x{=}L,t)/\partial x = 0$ at $x = L$). The tip of the filopodia is free to move at a velocity of $V = 3\ \mu m\,min^{-1}$ (moving boundary condition). The numerical values of other parameters in the model have been determined experimentally:[250] $k_{on} = 0.8\ \mu M^{-1}s^{-1}$ and $k_{off} = 0.12\ s^{-1}$ ($k_{off} = 0\ s^{-1}$ if the binding were irreversible); the diffusion coefficient of fascin is $D = 6 \times 10^{-8}\ cm^2 s^{-1}$. The results of the model are summarized in Figure 18c, in which the percentages of cross-linked actin is plotted for the shorter (3 μm) and for the longer (10 μm) filopodia. In the former case, the fascin cross-linker can reach the tip of the filopodium with either reversible or irreversible binding. When, however, the filopodium is long, reversible fascin–actin binding based on RD is required to ensure that all the filopodium is polymerized and mechanically strengthened.

4.3.3. Choosing Direction: Gradient Sensing and Cell Polarization

So far, we have seen how RD helps maintain a motile cell on its course, but we have not investigated why and how the cell decides to migrate in a given direction. The answer lies in the ability of the cell to respond to external gradients of chemoattractant molecules—significantly, by means that are very different and more complex than those used by prokaryotes (see Section 3.1). A case in point is fast moving eukaryotic cells, such as neutrophils and cells of social amoeba *Dictyostelium discoideum*, which are remarkable for sensing and moving up very shallow spatial gradients (ca. 2–10% concentration difference across the length of the cell).[251,252] The gradient stimulates activation of cell-surface receptors (G-protein coupled receptors) which are initially distributed uniformly along the perimeter of the cell. Activation of the receptor recruits phosphatidylinositol 3-kinase (PI3K) to the membrane where it phosphorylates PI(3,4,5)P$_2$ to generate PI(3,4,5)P$_3$ (a membrane phospholipid phosphorylated at position 3′ on the inositol head group). During this initial stage of chemotaxis, commonly referred to as gradient sensing (Figure 19a), PIP$_3$-binding proteins rapidly ($t \approx 5$–10 s) localize to the part of the membrane facing the steepest gradient of chemoattractant[253] (henceforth this will be referred to as the cell front). This is accompanied by the localization of the PTEN enzyme, which degrades PIP$_3$ toward the back of the cell. The net result of these processes is the effective amplification of the shallow external gradient
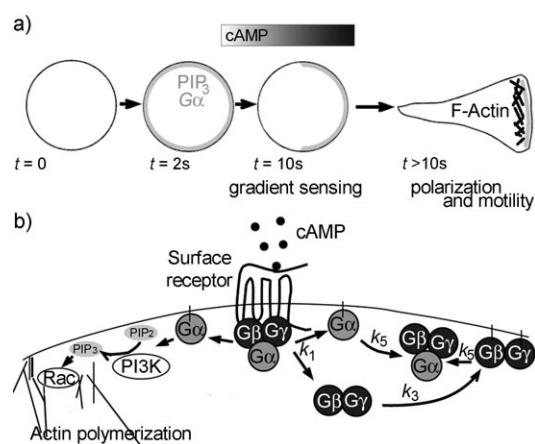

Figure 19. Gradient sensing and polarization in eukaryotic chemotaxis. a) The eukaryotic cell converts a shallow gradient of chemoattractant (here, cyclic AMP; dark gray represents a high concentration) into a sharp difference of molecular components at its front and rear. PIP$_3$ and G-protein Gα are in gray; F-actin is in black. b) Scheme of the relevant signaling events at the cell front that upon activation of cell-surface receptors (here, G-protein coupled receptors) by the chemoattractant (cAMP) lead to polarization of the cell. Left: PI3K is recruited to the front membrane where it generates PIP$_3$, which then recruits RacGTPase and initiates localized polymerization of actin. Right: a schematic depiction of the proposed molecular components in a balanced inactivation model. Here, Gα corresponds to the activator *A* (and also to the component of the gray front in (a)), and the Gβ-Gγ complex to the inhibitor species *I*. The important feature of this model is that Gβ-Gγ can associate with the membrane to form additional membrane-bound inhibitor. This membrane-bound inhibitor is mutually inhibitory with Gα as they form a tertiary complex consisting of all three G-proteins. The postulated involvement of Gα, Gβ, and Gγ in this process has not yet been verified in experiments.

being sensed into a steep/"polarized" distribution of the membrane and associated proteins such that the front and the back regions of the cell become biochemically and functionally distinct (see Ref. [254] for a discussion of the specific proteins involved). Importantly, the PIP$_3$ at the front of the cell recruits Rac GTPase, which promotes localized polymerization of actin, membrane protrusion, and, ultimately, cell movement towards the higher concentration of the chemoattractant (Figure 19).

A number of mathematical models have described the internal signaling/motility machinery of the cell as a reaction-diffusion system to explain the amplification of an external gradient and concomitant sharp front/rear segregation of molecular components, (see the reviews in Refs. [253,254]). Most of these models have been based on the Turing-like activator-inhibitor dynamics[67–70,255,256] we have seen in Section 2. One of the simplest formulations, called LEGI (local excitation-global inhibition), proposes that intracellular response to external gradients is regulated by the simultaneous production of two secondary messengers whose concentrations are proportional to the fraction of surface receptors *S* activated by the chemoattractant at each point on the membrane. These messengers are 1) a slowly diffusing signaling activator *A* generated at and confined to the membrane[252,257,258] (some examples are G-proteins and

4190 www.angewandte.org

© 2010 Wiley-VCH Verlag GmbH & Co. KGaA, Weinheim

Angew. Chem. Int. Ed. **2010**, *49*, 4170–4198

PIP$_3$) and 2) a locally generated inhibitor I which is free to diffuse rapidly through the cell (the identity of inhibitors is experimentally unproven and thus controversial, although various candidate molecules and even mechanisms have been proposed[254,256,259–263]). The net response of the cell is then determined by the concentration of membrane-bound species R ("response element") which is activated by A and deactivated by I, and its role is to activate/control downstream components of the motility machinery (for example, Rac). The overall "wiring scheme" of the model is illustrated in Figure 20a, and translates into RD Equations (20)–(22) (see also Ref. [264]).

$$\frac{\partial A}{\partial t} = k_1 S - k_2 A \qquad (20)$$

$$\frac{\partial I}{\partial t} = D\nabla^2 I + k_3 S - k_4 I \qquad (21)$$

$$\frac{\partial R}{\partial t} = k_5 A - k_6 I R \qquad (22)$$

Here, k_i ($i = 1$ to 6) are rate constants and D is the diffusion coefficient of I. Figure 20b and Figure 20c show the steady-state solution for the distribution of I and R along the perimeter of the cell (approximated as a circle). Although the model reproduces the polarized response of the cell as well as several other experimental observations,[265] its major shortcoming is that the internal gradients that emerge are not steeper than the external gradient of the chemoattractant—in other words, no effective amplification is observed.[266,267]

To achieve this amplification effect, the LEGI has been extended to the so-called balanced inactivation (BI) model.[261] Here, as in LEGI, the concentration S of the receptors on the surface of the cell is proportional to the concentration of the chemoattractant at a given location of the membrane. The activated receptors, in turn, control the production (with the rate constants assumed to be the same, k_1) of the membrane-bound activator A and the cytosolic inhibitor I_c. The latter can diffuse through the cytoplasm with diffusion coefficient D and can attach to the membrane with rate k_3 to create I. The reaction scheme for these events is shown in Figure 20d and the pertinent RD equations are Equations (23)–(25).

$$\frac{\partial A}{\partial t} = k_1 S - k_2 A - k_5 A I \qquad (23)$$

$$\frac{\partial I}{\partial t} = k_3 I_c - k_4 I - k_5 A I \qquad (24)$$

$$\frac{\partial I_c}{\partial t} = D\nabla^2 I_c \qquad (25)$$

The rate constants k_2 and k_4 describe spontaneous but slow degradation of A and I, respectively, and k_5 describes a reaction in which A and I are mutually inhibitory. For the boundary conditions, the flux of I_c through the membrane (per unit area) is given as $-D\partial I_c/\partial n = k_3 I_c - k_1 S$, where the left-hand side of the equation reflects the amount of I_c leaving the cytoplasm (n defines the outward normal to the mem-
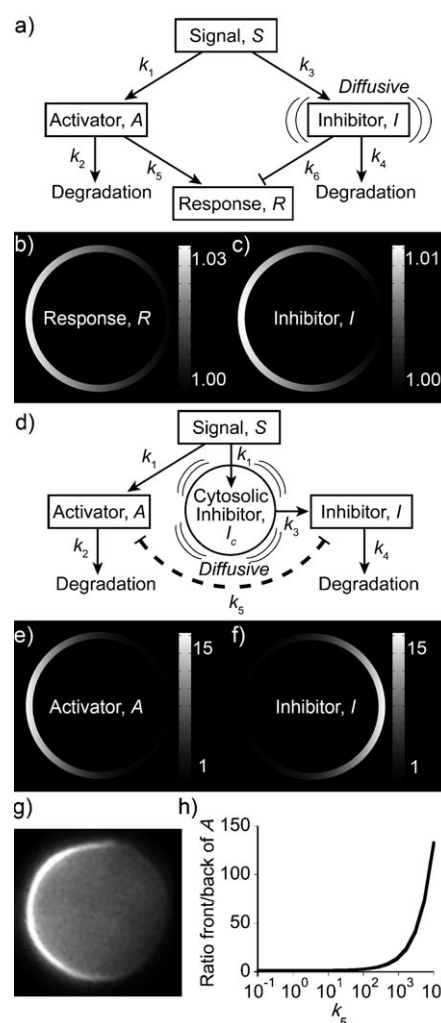

Figure 20. Comparison of the local excitation-global inhibition (LEGI) and the balanced inactivation (BI) models of gradient sensing. a) Schematic representation of LEGI. b,c) The steady-state, normalized concentration profiles of the response element R and the inhibitor I calculated by the LEGI model. The solution demonstrates that R responds and polarizes the cell in the direction of the applied chemoattractant (from the left side of the picture), albeit with a small gradient R between the "front" and "back" (ca. 1.03 times). Parameters used in the calculations: $D = 1 \times 10^{-8}$ cm^2 s^{-1}, $k_1 = k_3 = k_5 = 0.1$ s^{-1}, $k_2 = k_4 = 0.02$ s^{-1}, and $k_6 = 0.02$ m^2 mol^{-1} s^{-1}). d) Schematic representation of the BI model. e,f) The concentration profile for the activator A (which in this model also plays the role of R) and the membrane-bound form of the inhibitor I. The mutual inhibition of A and I results in the concentration profiles of these species being spatially separated, and the "contrast"/amplification between the front and the back regions is high. Parameters used in the calculations: $D = 1 \times 10^{-6}$ cm^2 s^{-1}, $k_1 = 1$ s^{-1}, $k_2 = k_4 = 0.2$ s^{-1}, $k_3 = 3$ μm s^{-1}, and $k_5 = 1000$ μm^2 mol^{-1} s^{-1}). g) Representative experimental image (from Ref. [266] with permission) of the localization of the GFP-tagged PIP3-binding proteins in a chemoattractant-stimulated environment (the cell is rounded because of the presence of the actin depolymerizing drug Latrunculin A; under these conditions, the gradient sensing response remains intact). h) The ratio of the concentrations of A at the "front" to that at the "back" of the cell plotted as a function of the rate constant k_5 and calculated according to the BI model. This plot demonstrates that the reaction term representing mutual inhibition between A and I ($k_5 A I$) is crucial for the amplification of the external gradients—when k_5 is small, no amplification is observed.

brane's surface). The first term on the right accounts for the conversion of I_c into I [compare with Eq. (24)], and the second term for the production of I_c by activated receptors S. Unlike in LEGI, A plays the role of both the activator and the response element necessary to influence downstream species.

When solved numerically, the BI model predicts a highly asymmetric distribution of A and a 100-fold overall amplification of the external gradient. Curiously, this is achieved despite the apparent similarity of the BI equations to LEGI. The key difference, however, is the additional reaction term $-k_5 A I$ in both Equations (23) and (24) [analogous to the term $-k_6 I R$ in Eq. (22) of LEGI, but not found in Eq. (21)]. This term represents the "cross-talk" and mutual inhibition between A and I (see dashed line in Figure 20d) and effectively causes these species to separate into different regions of the membrane, with A near the front and I near the back of the cell. Consequently, if the cross-talk is efficient (that is, k_5 is high, above 100 $\mu m^2 mol^{-1} s^{-1}$), the ratios of the front-to-back concentrations of A can be as high as 15:1. This is over two orders of magnitude larger than the original chemoattractant gradient (only ca. 5% difference in the concentration across the cell length). We see once again how the introduction of a single nonlinear term into a set of RD equations can cause rather dramatic changes in the model's predictions.

Finally, a word of caution is necessary—although the results outlined in this section are very much in line with experiments, it should be remembered that the nature of the inhibitors I stipulated in both BI and LEGI is still unknown (see Figure 19b). This is certainly a weak point of the models, but it also offers some exciting opportunities for future research, since unequivocal confirmation of the existence and the nature of the inhibitors would be one of the rare examples where theory precedes experiment. It would also be a testament to the power of RD modeling as an a priori rather than a posteriori tool with which to study cell behavior.
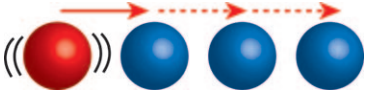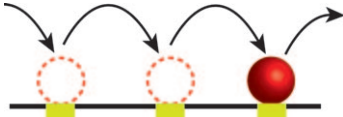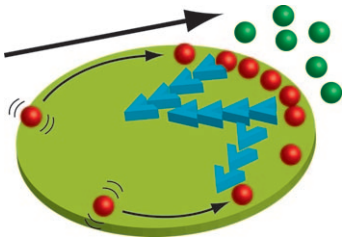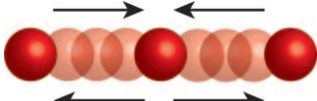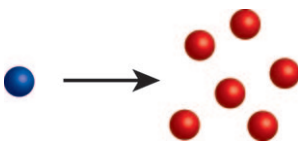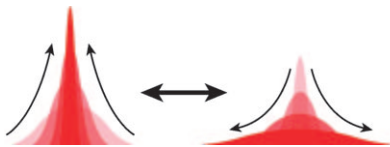
5. Conclusions and Outlook

Throughout this Review, we have strived to illustrate that reaction-diffusion processes are an important component of intracellular transport and control. One of the reasons for their preponderance is that they are energetically less costly than active transport. For this reason, not only the small and simple prokaryotes but also the larger and more complex eukaryotes use RD; otherwise, these cells would simply not be able to pay the high "energy bill" for moving their constituent parts around by active transport. Of course, processes based on diffusion are slow, especially if the distances involved become large. To cope with diffusional limitations, cells have designed several RD "motifs/mechanisms" in which the skillful coupling of diffusion with reaction and/or with the dimensionality of the system makes the overall process more efficient and shortens the delivery time. We have seen several such motifs: reduction of dimensionality (for example, in the targeting of DNA sites by proteins and in signaling cascades), domino-like activation patterns (for example, in kinase signaling and in lateral phosphoryla-

tion propagation), extension of gradients by complexation (for example, as in Ran-GTP complexation during mitotic spindle assembly), and the amplification of gradients by activator-inhibitor coupling (e.g., in cell polarization). These and some other motifs are summarized in Table 2. Assuming that over the course of evolution nature has selected these motifs for optimal functioning (in terms of delivery speeds, signaling rates, etc.), we believe that they provide a blueprint for the construction of artificial RD systems[268] of the future. While the field of systems chemistry[29–33] is only in its infancy, it will, at least in our opinion, soon be a mainstream area of chemical research.

For understanding and synthesizing systems of concerted reactions, the involvement of migrating chemicals seems not only a logical extension of the present one-reaction-in-one-pot paradigm, but is also a route to chemical systems that could adapt to environmental changes, sense and amplify signals, self-propel, self-heal, or maybe even self-replicate. In this quest for "artificial cells", the real cellular RD systems can provide inspiration and guidance. Although the development of such systems is certainly not going to be a trivial affair, it is certainly possible, as already evidenced by the generic schemes developed recently for the rational design of RD systems including Turing patterns[269–273] or periodic precipitation reactions.[274]

We close with some general observations we made while preparing this Review. The first one is that diffusion is not at all a boring subject typically associated with "smearing-up" concentration gradients and with wasteful dissipation of chemical energy. When properly synchronized with chemical reactions, it can become a purposeful and powerful tool with which to transport, position, and control small structures. In doing so, it can be amazingly precise—take, for example, the Min system, where RD places the Z ring with a precision of approximately 1% of the cell's length (tens of nanometers!). The second, and related point is that we are only beginning to learn about the astounding prowess and richness of cellular phenomena stemming from RD. While the macroscopic RD systems, such as Turing or BZ patterns, have been studied for decades, many of the publications on cellular RD that we have cited in this Review are quite recent, which suggests that this area of study is taking off. As the resolution of in-cell microscopy techniques[12–17,275] improves, one might expect that more and more researchers will be able to track the paths of molecules within cells, and more RD processes are likely to be discovered. It should be pointed out, however, that for this study to become science (rather than Lord Rutherford's "stamp-collecting"[276]), experiments must go hand-in hand with theory. Reaction diffusion is simply too complex and counterintuitive to understand without mathematical models. Fortunately, the construction and solution of RD equations follows well-defined rules, some of which we hope to have expounded in this Review; more information on the mathematics of RD can be found in recent monographs on the subject.[64,71,277] Overall, further journey into the realm of cellular RD might not necessarily be easy and might require a combination of tools from various disciplines (chemistry, cell biology, imaging, mathematics, physics), but it certainly promises to be a great adventure.

4192   www.angewandte.org

© 2010 Wiley-VCH Verlag GmbH & Co. KGaA, Weinheim

Angew. Chem. Int. Ed. **2010**, *49*, 4170–4198

Table 2: Common "motifs" in intracellular reaction diffusion.

Description		Examples	Section	Function
reduction of dimensionality		● targeting of specific sites on DNA by proteins (3D→1D)[121, 123, 125]	3.3	speeds up targeting or increases depth of penetration into cell
		● changes in cell shape (3D→2D)[74]	4.1.1	
domino-like relay		● kinase signaling cascades[164]	4.1.1	accelerates signal transduction, amplifies signals
		● lateral propagation of receptor activation on the cell membrane[166]	4.1.1	
		● calcium waves[176, 180, 186, 289]	4.1.2	
gradient extension by complexation		● Ran-GTP gradients[162, 202, 203, 290]	4.2	extends the "reach" of complexed chemicals
molecular transport by reversible binding		● cross-linking of actin by fascin in filopodia[250]	4.3.2	cross-links and strengthens filopodia
directional cell response through polarization		● gradient sensing[253, 261, 267]	4.3.3	protrusion and directed motility along chemoattractant gradients
		● actin treadmill[228, 229, 291]	4.3.1	
spatial or temporal oscillations		● Min system[114, 116, 118]	3.2	precise positioning of cellular structures; frequency-specific responses
		● calcium oscillations[165, 169, 174, 268]	4.1.2	
amplification of signals		● gradient sensing[253, 261, 267]	4.3.3	sensing of chemoattractants
positive and negative feedback		● filopodia and membrane waves[242–244]	4.3.2	toggling between different functional states

[1] B. N. Kholodenko, W. Kolch, *Cell* **2008**, *133*, 566.
[2] O. Shimomura, F. H. Johnson, Y. Saiga, *J. Cell. Comp. Physiol.* **1962**, *59*, 223.

[3] M. Chalfie, Y. Tu, G. Euskirchen, W. W. Ward, D. C. Prasher, *Science* **1994**, *263*, 802.

[4] R. Heim, D. C. Prasher, R. Y. Tsien, *Proc. Natl. Acad. Sci. USA* **1994**, *91*, 12501.

[5] O. Shimomura, *Angew. Chem.* **2009**, *121*, 5698; *Angew. Chem. Int. Ed.* **2009**, *48*, 5590.

[6] M. Chalfie, *Angew. Chem.* **2009**, *121*, 5711; *Angew. Chem. Int. Ed.* **2009**, *48*, 5603.

[7] R. Y. Tsien, *Angew. Chem.* **2009**, *121*, 5721; *Angew. Chem. Int. Ed.* **2009**, *48*, 5612.

[8] E. A. Jares-Erijman, T. M. Jovin, *Nat. Biotechnol.* **2003**, *21*, 1387.

[9] P. Atkins, J. de Paula, *Physical Chemistry*, 7th ed., W. H. Freeman, New York, **2001**.

[10] I. Levine, *Physical Chemistry*, 6th ed., McGraw-Hill, New York, **2008**.

[11] D. A. McQuarrie, J. D. Simon, *Physical Chemistry: A Molecular Approach*, University Science Books, Sausalito, **1997**.

[12] B. Huang, W. Q. Wang, M. Bates, X. W. Zhuang, *Science* **2008**, *319*, 810.

[13] M. J. Rust, M. Bates, X. W. Zhuang, *Nat. Methods* **2006**, *3*, 793.

[14] S. W. Hell, *Nat. Biotechnol.* **2003**, *21*, 1347.

[15] S. W. Hell, *Science* **2007**, *316*, 1153.

[16] E. Betzig, G. H. Patterson, R. Sougrat, O. W. Lindwasser, S. Olenych, J. S. Bonifacino, M. W. Davidson, J. Lippincott-Schwartz, H. F. Hess, *Science* **2006**, *313*, 1642.

[17] M. G. L. Gustafsson, *Proc. Natl. Acad. Sci. USA* **2005**, *102*, 13081.

[18] N. J. Durr, T. Larson, D. K. Smith, B. A. Korgel, K. Sokolov, A. Ben-Yakar, *Nano Lett.* **2007**, *7*, 941.

[19] C. Sönnichsen, A. P. Alivisatos, *Nano Lett.* **2005**, *5*, 301.

[20] H. F. Wang, T. B. Huff, D. A. Zweifel, W. He, P. S. Low, A. Wei, J. X. Cheng, *Proc. Natl. Acad. Sci. USA* **2005**, *102*, 15752.

[21] J. Chen, et al., *Nano Lett.* **2005**, *5*, 473.

[22] J. Y. Chen, et al., *Adv. Mater.* **2005**, *17*, 2255.

[23] M. F. Kircher, U. Mahmood, R. S. King, R. Weissleder, L. Josephson, *Cancer Res.* **2003**, *63*, 8122.

[24] J. W. M. Bulte, D. L. Kraitchman, *NMR Biomed.* **2004**, *17*, 484.

[25] M. Zhao, D. A. Beauregard, L. Loizou, B. Davletov, K. M. Brindle, *Nat. Med.* **2001**, *7*, 1241.

[26] W. C. W. Chan, D. J. Maxwell, X. H. Gao, R. E. Bailey, M. Y. Han, S. M. Nie, *Curr. Opin. Biotechnol.* **2002**, *13*, 40.

[27] P. Mitchell, *Nat. Biotechnol.* **2001**, *19*, 1013.

[28] E. Klarreich, *Nature* **2001**, *413*, 450.

[29] R. F. Ludlow, S. Otto, *Chem. Soc. Rev.* **2008**, *37*, 101.

[30] N. Wagner, G. Ashkenasy, *Chem. Eur. J.* **2009**, *15*, 1765.

[31] Z. Dadon, N. Wagner, G. Ashkenasy, *Angew. Chem.* **2008**, *120*, 6221; *Angew. Chem. Int. Ed.* **2008**, *47*, 6128.

[32] A. Hjelmfelt, E. D. Weinberger, J. Ross, *Proc. Natl. Acad. Sci. USA* **1991**, *88*, 10983.

[33] A. Arkin, J. Ross, *Biophys. J.* **1994**, *67*, 560.

[34] H. Lodish, A. Berk, P. Matsudaira, C. A. Kaiser, M. Krieger, M. P. Scott, S. L. Zipursky, J. Darnell, *Molecular Cell Biology*, 5th ed., W. H. Freeman, New York, **2004**.

[35] a) J. D. Murray, *Mathematical Biology: An Introduction*, Vol. 1, 3rd ed., Springer, New York, 2002; b) J. D. Murray, *Mathematical Biology: Spatial Models and Biomedical Applications*, Vol. 2, 3rd ed., Springer, New York, **2003**.

[36] a) B. A. Grzybowski, K. J. M. Bishop, C. J. Campbell, M. Fialkowski, S. K. Smoukov, *Soft Matter* **2005**, *1*, 114; b) N. F. Britton, *Reaction-Diffusion Equations and Their Applications to Biology*, Academic Press, London, 1986; c) P. Gray, S. K. Scott, *Chemical Oscillations and Instabilities: Non-linear Chemical Kinetics*, Oxford University Press, New York, 1990; d) G. Nicolis, I. Prigogine, *Self-organization in Nonequilibrium Systems*, John Wiley & Sons, New York, **1977**.

[37] A. N. Zaikin, A. M. Zhabotinsky, *Nature* **1970**, *225*, 535.

[38] R. J. Field, M. Burger, *Oscillations and Traveling Waves in Chemical Systems*, Wiley, New York, **1985**.

[39] a) K. J. M. Bishop, B. A. Grzybowski, *Phys. Rev. Lett.* **2006**, *97*, 128702; b) K. J. M. Bishop, M. Fialkowski, B. A. Grzybowski, *J. Am. Chem. Soc.* **2005**, *127*, 15943.

[40] P. M. Wood, J. Ross, *J. Chem. Phys.* **1985**, *82*, 1924.

[41] A. Hanna, A. Saul, K. Showalter, *J. Am. Chem. Soc.* **1982**, *104*, 3838.

[42] P. De Kepper, I. R. Epstein, K. Kustin, M. Orban, *J. Phys. Chem.* **1982**, *86*, 170.

[43] J. Ross, S. C. Muller, C. Vidal, *Science* **1988**, *240*, 460.

[44] V. K. Vanag, L. F. Yang, M. Dolnik, A. M. Zhabotinsky, I. R. Epstein, *Nature* **2000**, *406*, 389.

[45] K. J. Lee, W. D. McCormick, Q. Ouyang, H. L. Swinney, *Science* **1993**, *261*, 192.

[46] G. Ertl, *Science* **1991**, *254*, 1750.

[47] J. Wolff, A. G. Papathanasiou, I. G. Kevrekidis, H. H. Rotermund, G. Ertl, *Science* **2001**, *294*, 134.

[48] R. E. Liesegang, *Naturwiss. Wochenschr.* **1896**, *10*, 353.

[49] B. Chopard, P. Luthi, M. Droz, *Phys. Rev. Lett.* **1994**, *72*, 1384.

[50] a) M. Fialkowski, A. Bitner, B. A. Grzybowski, *Phys. Rev. Lett.* **2005**, *94*, 018303; b) I. T. Bensemann, M. Fialkowski, B. A. Grzybowski, *J. Phys. Chem. B* **2005**, *109*, 2774; c) I. Lagzi, B. Kowalczyk, B. A. Grzybowski, *J. Am. Chem. Soc.* **2010**, *132*, 58.

[51] M. Flicker, J. Ross, *J. Chem. Phys.* **1974**, *60*, 3458.

[52] S. C. Müller, J. Ross, *J. Phys. Chem. A* **2003**, *107*, 7997.

[53] E. Ammelt, D. Schweng, H. G. Purwins, *Phys. Lett. A* **1993**, *179*, 348.

[54] E. L. Gurevich, A. L. Zanin, A. S. Moskalenko, H. G. Purwins, *Phys. Rev. Lett.* **2003**, *91*, 154501.

[55] P. J. Heaney, A. M. Davis, *Science* **1995**, *269*, 1562.

[56] M. B. Short, J. C. Baygents, J. W. Beck, D. A. Stone, R. S. Toomey, R. E. Goldstein, *Phys. Rev. Lett.* **2005**, *94*, 018501.

[57] *Glossary of Geology*, 3rd ed., American Geological Institute, Alexandria, **1987**.

[58] E. O. Budrene, H. C. Berg, *Nature* **1991**, *349*, 630.

[59] E. O. Budrene, H. C. Berg, *Nature* **1995**, *376*, 49.

[60] B. Hess, *Naturwissenschaften* **2000**, *87*, 199.

[61] A. T. Winfree, *The Geometry of Biological Time*, 2nd ed., Springer, New York, **2001**.

[62] S. Kondo, R. Asai, *Nature* **1995**, *376*, 765.

[63] T. X. Jiang, R. B. Widelitz, W. M. Shen, P. Will, D. Y. Wu, C. M. Lin, H. S. Jung, C. M. Chuong, *Int. J. Dev. Biol.* **2004**, *48*, 117.

[64] W. M. Deen, *Analysis of Transport Phenomena*, Oxford University Press, New York, **1998**.

[65] N. G. Van Kampen, *Stochastic Processes in Physics and Chemistry*, Elsevier Science Publishers, New York, **1981**.

[66] R. Metzler, J. Klafter, *Phys. Rep.* **2000**, *339*, 1.

[67] A. M. Turing, *Philos. Trans. R. Soc. London* **1952**, *237*, 37.

[68] T. Miura, T. Matsumoto, *Proc. R. Soc. London* **2000**, *267*, 1185.

[69] T. Miura, *Insectes Soc.* **2001**, *48*, 216.

[70] F. Siegert, C. J. Weijer, *Curr. Biol.* **1995**, *5*, 937.

[71] B. A. Grzybowski, *Chemistry in Motion: Reaction-Diffusion Systems for Micro- and Nanotechnology*, Wiley, Chichester, UK, **2009**.

[72] M. B. Elowitz, M. G. Surette, P. E. Wolf, J. B. Stock, S. Leibler, *J. Bacteriol.* **1999**, *181*, 197.

[73] R. Swaminathan, C. P. Hoang, A. S. Verkman, *Biophys. J.* **1997**, *72*, 1900.

[74] J. Meyers, J. Craig, D. J. Odde, *Curr. Biol.* **2006**, *16*, 1685.

[75] B. Alberts, A. Johnson, J. Lewis, M. Raff, K. Roberts, P. Walter, *Molecular Biology of the Cell*, 4th ed., Garland Science, New York, **2002**.

[76] J. Howard, *Annu. Rev. Physiol.* **1996**, *58*, 703.

[77] J. S. Lee, M. S. Mayes, M. H. Stromer, C. G. Scanes, S. Jeftinija, L. L. Anderson, *Exp. Biol. Med.* **2004**, *229*, 632.

[78] I. Wacker, C. Kaether, A. Kromer, A. Migala, W. Almers, H. H. Gerdes, *J. Cell Sci.* **1997**, *110*, 1453.

[79] O. Culic, M. L. H. Gruwel, J. Schrader, *Am. J. Physiol.* **1997**, *273*, C205.

[80] S. Ghaemmaghami, W. Huh, K. Bower, R. W. Howson, A. Belle, N. Dephoure, E. K. O'Shea, J. S. Weissman, *Nature* **2003**, *425*, 737.

[81] P. Giannakakou, D. L. Sackett, Y. Ward, K. R. Webster, M. V. Blagosklonny, T. Fojo, *Nat. Cell Biol.* **2000**, *2*, 709.

[82] V. Prahlad, B. T. Helfand, G. M. Langford, R. D. Vale, R. D. Goldman, *J. Cell Sci.* **2000**, *113*, 3939.

[83] Y. Mimori-Kiyosue, N. Shiina, S. Tsukita, *J. Cell Biol.* **2000**, *148*, 505.

[84] S. Y. Trostel, D. L. Sackett, T. Fojo, *Cell Cycle* **2006**, *5*, 2253.

[85] E. C. Garner, C. S. Campbell, R. D. Mullins, *Science* **2004**, *306*, 1021.

[86] E. C. Garner, C. S. Campbell, D. B. Weibel, R. D. Mullins, *Science* **2007**, *315*, 1270.

[87] D. Popp, A. Yamamoto, M. Iwasa, A. Narita, K. Maeda, Y. Maeda, *Biochem. Biophys. Res. Commun.* **2007**, *353*, 109.

[88] J. Møller-Jensen, J. Borch, M. Dam, R. B. Jensen, P. Roepstorff, K. Gerdes, *Mol. Cell* **2003**, *12*, 1477.

[89] M. A. Fogel, M. K. Waldor, *Genes Dev.* **2006**, *20*, 3269.

[90] J. Møller-Jensen, R. B. Jensen, K. Gerdes, *Trends Microbiol.* **2000**, *8*, 313.

[91] D. A. Mohl, J. W. Gober, *Cell* **1997**, *88*, 675.

[92] K. Gerdes, J. Møller-Jensen, R. B. Jensen, *Mol. Microbiol.* **2000**, *37*, 455.

[93] A. M. Stock, V. L. Robinson, P. N. Goudreau, *Annu. Rev. Biochem.* **2000**, *69*, 183.

[94] J. A. Hoch, *Curr. Opin. Microbiol.* **2000**, *3*, 165.

[95] H. C. Berg, E. M. Purcell, *Biophys. J.* **1977**, *20*, 193.

[96] G. H. Wadhams, J. P. Armitage, *Nat. Rev. Mol. Cell Biol.* **2004**, *5*, 1024.

[97] J. R. Maddock, L. Shapiro, *Science* **1993**, *259*, 1717.

[98] S. Khan, J. L. Spudich, J. A. McCray, D. R. Trentham, *Proc. Natl. Acad. Sci. USA* **1995**, *92*, 9757.

[99] J. E. Segall, M. D. Manson, H. C. Berg, *Nature* **1982**, *296*, 855.

[100] J. E. Segall, A. Ishihara, H. C. Berg, *J. Bacteriol.* **1985**, *161*, 51.

[101] C. J. Camacho, S. R. Kimura, C. DeLisi, S. Vajda, *Biophys. J.* **2000**, *78*, 1094.

[102] T. A. J. Duke, N. Le Novere, D. Bray, *J. Mol. Biol.* **2001**, *308*, 541.

[103] P. Cluzel, M. Surette, S. Leibler, *Science* **2000**, *287*, 1652.

[104] K. Lipkow, S. S. Andrews, D. Bray, *J. Bacteriol.* **2005**, *187*, 45.

[105] U. Alon, M. G. Surette, N. Barkai, S. Leibler, *Nature* **1999**, *397*, 168.

[106] G. Almogy, L. Stone, N. Ben-Tal, *Biophys. J.* **2001**, *81*, 3016.

[107] A. Vaknin, H. C. Berg, *Proc. Natl. Acad. Sci. USA* **2004**, *101*, 17072.

[108] E. Bi, J. Lutkenhaus, *Nature* **1991**, *354*, 161.

[109] F. J. Trueba, *Arch. Microbiol.* **1982**, *131*, 55.

[110] M. Howard, A. D. Rutenberg, S. de Vet, *Phys. Rev. Lett.* **2001**, *87*, 278102.

[111] H. Meinhardt, P. A. J. de Boer, *Proc. Natl. Acad. Sci. USA* **2001**, *98*, 14202.

[112] K. Kruse, *Biophys. J.* **2002**, *82*, 618.

[113] M. Howard, A. D. Rutenberg, *Phys. Rev. Lett.* **2003**, *90*, 128102.

[114] K. C. Huang, Y. Meir, N. S. Wingreen, *Proc. Natl. Acad. Sci. USA* **2003**, *100*, 12724.

[115] R. V. Kulkarni, K. C. Huang, M. Kloster, N. S. Wingreen, *Phys. Rev. Lett.* **2004**, *93*, 228103.

[116] D. M. Raskin, P. A. J. de Boer, *Proc. Natl. Acad. Sci. USA* **1999**, *96*, 4971.

[117] H. Zhou, J. Lutkenhaus, *J. Bacteriol.* **2003**, *185*, 4326.

[118] J. Lutkenhaus, *Annu. Rev. Biochem.* **2007**, *76*, 539.

[119] L. Romberg, P. A. Levin, *Annu. Rev. Microbiol.* **2003**, *57*, 125.

[120] The model discussed in the text relies entirely on experimentally verified (in vitro) molecular interactions. In addition to the positioning of the FtsZ ring, this model reproduces several other experimental observations, including the oscillation period of ca. 40 s, zebra-striped oscillations in filamentous cells, or oscillations in both rod-shaped and round cells (Ref. [114] and K. C. Huang, N. S. Wingreen, *Phys. Biol.* **2004**, *1*, 229). Earlier models of the Min system often make unrealistic assumptions such as continuous synthesis and degradation of Min proteins (Ref. [111]), although it has been proven experimentally that blocking this synthesis does not affect the oscillations (Ref. [116]). More recent models assume that the amounts of MinD and MinE proteins are conserved (this assumption is also used in the model discussed in the main text), and also attempt to provide a more detailed description of the underlying molecular interactions, including stochastic effects (for example, R. A. Kerr, H. Levine, T. J. Sejnowski, W. J. Rappel, *Proc. Natl. Acad. Sci. USA* **2006**, *103*, 347, and N. Pavin, H. C. Paljetak, V. Krstic, *Phys. Rev. E* **2006**, *73*, 021904). The reader is referred to an excellent review (K. Kruse, M. Howard, W. Margolin, *Mol. Microbiol.* **2007**, *63*, 1279) which compares these and other models. Interestingly, it has also been proposed that the positioning of the FtsZ ring is Min-independent and can be due to the so-called "nucleoid occlusion" (C. L. Woldringh, E. Mulder, J. A. C. Valkenburg, F. B. Wientjes, A. Zaritsky, N. Nanninga, *Res. Microbiol.* **1990**, *141*, 39). However, experiments with anucleate cells (cells with no chromosomes) show that the FtsZ ring still forms in the middle of the cell (Q. Sun, X. C. Yu, W. Margolin, *Mol. Microbiol.* **1998**, *29*, 491). Therefore, this mechanism appears important only for cells lacking the Min system (W. Margolin, *Nat. Rev. Mol. Cell Biol.* **2005**, *6*, 862).

[121] T. Hu, B. I. Shklovskii, *Phys. Rev. E* **2006**, *74*, 021903.

[122] M. Ptashne, A. Gann, *Essays Biochem.* **2001**, *37*, 1.

[123] K. V. Klenin, H. Merlitz, J. Langowski, C. X. Wu, *Phys. Rev. Lett.* **2006**, *96*, 018104.

[124] P. H. von Hippel, *Annu. Rev. Biophys. Biomol. Struct.* **2007**, *36*, 79.

[125] J. Widom, *Proc. Natl. Acad. Sci. USA* **2005**, *102*, 16909.

[126] A. D. Riggs, S. Bourgeois, M. Cohn, *J. Mol. Biol.* **1970**, *53*, 401.

[127] S. E. Halford, J. F. Marko, *Nucleic Acids Res.* **2004**, *32*, 3040.

[128] Y. M. Wang, R. H. Austin, E. C. Cox, *Phys. Rev. Lett.* **2006**, *97*, 048302.

[129] D. M. Gowers, G. G. Wilson, S. E. Halford, *Proc. Natl. Acad. Sci. USA* **2005**, *102*, 15883.

[130] B. van den Broek, M. A. Lomholt, S. M. J. Kalisch, R. Metzler, G. J. L. Wuite, *Proc. Natl. Acad. Sci. USA* **2008**, *105*, 15738.

[131] C. Bustamante, M. Guthold, X. S. Zhu, G. L. Yang, *J. Biol. Chem.* **1999**, *274*, 16665.

[132] N. Shimamoto, *J. Biol. Chem.* **1999**, *274*, 15293.

[133] O. Givaty, Y. Levy, *J. Mol. Biol.* **2009**, *385*, 1087.

[134] An interesting variant of the jumping mechanism is observed in proteins having more than one DNA binding domain (S. E. Halford, D. M. Gowers, R. B. Sessions, *Nat. Struct. Biol.* **2000**, *7*, 705), for example, the V-shaped Lac repressor, whose two "tips" can bind to DNA and can thus bring together two distant DNA loci. When this happens, thermal fluctuations can mediate the so-called intersegmental transfer of the protein from one DNA segment to another (Ref. [136]). Similar to "jumping", this mechanism allows the protein to travel hundreds of base pairs away from its current site. However, while "jumping" involves dissociation of the protein from the DNA, the protein remains bound to the DNA during intersegmental transfer. Intersegmental transfer has been observed directly through scanning force microscopy (SFM) for *E. coli* RNA polymerase on DNA (Ref. [131]) and has also been

implicated to occur in the lac repressor (M. G. Fried, D. M. Crothers, *J. Mol. Biol.* **1984**, *172*, 263).

[135] R. H. Porecha, J. T. Stivers, *Proc. Natl. Acad. Sci. USA* **2008**, *105*, 10791.

[136] O. G. Berg, R. B. Winter, P. H. Von Hippel, *Biochemistry* **1981**, *20*, 6929.

[137] G. M. Viswanathan, S. V. Buldyrev, S. Havlin, M. G. E. da Luz, E. P. Raposo, H. E. Stanley, *Nature* **1999**, *401*, 911.

[138] F. Bartumeus, M. G. E. Da Luz, G. M. Viswanathan, J. Catalan, *Ecology* **2005**, *86*, 3078.

[139] G. M. Viswanathan, V. Afanasyev, S. V. Buldyrev, E. J. Murphy, P. A. Prince, H. E. Stanley, *Nature* **1996**, *381*, 413.

[140] F. Bartumeus, F. Peters, S. Pueyo, C. Marrase, J. Catalan, *Proc. Natl. Acad. Sci. USA* **2003**, *100*, 12771.

[141] M. A. Lomholt, T. Ambjornsson, R. Metzler, *Phys. Rev. Lett.* **2005**, *95*, 260603.

[142] M. D. Barkley, *Biochemistry* **1981**, *20*, 3833.

[143] B. F. Lang, M. W. Gray, G. Burger, *Annu. Rev. Genet.* **1999**, *33*, 351.

[144] W. Martin, B. Stoebe, V. Goremykin, S. Hansmann, M. Hasegawa, K. V. Kowallik, *Nature* **1998**, *393*, 162.

[145] L. Margulis, J. F. Stolz, *Adv. Space Res.* **1984**, *4*, 195.

[146] C. de Duve, *Sci. Am.* **1996**, *274*, 50.

[147] C. de Duve, *Nat. Rev. Genet.* **2007**, *8*, 395.

[148] D. H. Schott, R. N. Collins, A. Bretscher, *J. Cell Biol.* **2002**, *156*, 35.

[149] E. Mohr, *Prog. Neurobiol.* **1999**, *57*, 507.

[150] A. Bashirullah, R. L. Cooperstock, H. D. Lipshitz, *Annu. Rev. Biochem.* **1998**, *67*, 335.

[151] P. Lasko, *FASEB J.* **1999**, *13*, 421.

[152] K. L. Mowry, C. A. Cote, *FASEB J.* **1999**, *13*, 435.

[153] G. J. Bassell, Y. Oleynikov, R. H. Singer, *FASEB J.* **1999**, *13*, 447.

[154] J. H. Carson, S. J. Kwon, E. Barbarese, *Curr. Opin. Neurobiol.* **1998**, *8*, 607.

[155] J. O. Deshler, M. I. Highett, T. Abramson, B. J. Schnapp, *Curr. Biol.* **1998**, *8*, 489.

[156] M. L. King, Y. Zhou, M. Bubunenko, *Bioessays* **1999**, *21*, 546.

[157] O. Steward, *Neuron* **1997**, *18*, 9.

[158] P. A. Takizawa, A. Sil, J. R. Swedlow, I. Herskowitz, R. D. Vale, *Nature* **1997**, *389*, 90.

[159] Another motif commonly found in signaling pathways is composed of two forms of protein: an active one bound to GTP, and an inactive one bound to the GDP nucleotide. This convertible system is controlled by two types of proteins of "opposing" activities: GEF (guanine exchange factor) that catalyzes the GDP to GTP exchange, and the GTPase activating protein (GAP) that induces the hydrolysis of GTP to GDP.

[160] I. A. Yudushkin, A. Schleifenbaum, A. Kinkhabwala, B. G. Neel, C. Schultz, P. I. H. Bastiaens, *Science* **2007**, *315*, 115.

[161] G. C. Brown, B. N. Kholodenko, *FEBS Lett.* **1999**, *457*, 452.

[162] P. Bastiaens, M. Caudron, P. Niethammer, E. Karsenti, *Trends Cell Biol.* **2006**, *16*, 125.

[163] B. N. Kholodenko, *Trends Cell Biol.* **2002**, *12*, 173.

[164] B. N. Kholodenko, *Nat. Rev. Mol. Cell Biol.* **2006**, *7*, 165.

[165] N. I. Markevich, M. A. Tsyganov, J. B. Hoek, B. N. Kholodenko, *Mol. Syst. Biol.* **2006**, *2*, 8.

[166] C. Tischer, P. I. H. Bastiaens, *Nat. Rev. Mol. Cell Biol.* **2003**, *4*, 971.

[167] S. R. Hubbard, M. Mohammadi, J. Schlessinger, *J. Biol. Chem.* **1998**, *273*, 11987.

[168] P. J. Verveer, F. S. Wouters, A. R. Reynolds, P. I. H. Bastiaens, *Science* **2000**, *290*, 1567.

[169] G. Carpenter, K. J. Lembach, M. M. Morrison, S. Cohen, *J. Biol. Chem.* **1975**, *250*, 4297.

[170] D. Cuvelier, M. Thery, Y. S. Chu, S. Dufour, J. P. Thiery, M. Bornens, P. Nassoy, L. Mahadevan, *Curr. Biol.* **2007**, *17*, 694.

[171] J. Lechleiter, S. Girard, E. Peralta, D. Clapham, *Science* **1991**, *252*, 123.

[172] M. J. Berridge, *Nature* **1993**, *361*, 315.

[173] M. J. Berridge, *J. Exp. Biol.* **1997**, *200*, 315.

[174] S. A. Stricker, *Dev. Biol.* **1995**, *170*, 496.

[175] R. A. Fontanilla, R. Nuccitelli, *Biophys. J.* **1998**, *75*, 2079.

[176] T. Meyer, L. Stryer, *Annu. Rev. Biophys. Biophys. Chem.* **1991**, *20*, 153.

[177] J. D. Lechleiter, D. E. Clapham, *Cell* **1992**, *69*, 283.

[178] S. H. Strogatz, *Nonlinear Dynamics and Chaos: With Applications to Physics, Biology, Chemistry, and Engineering*, Perseus Books Publishing, Cambridge, **1994**.

[179] M. J. Berridge, M. D. Bootman, P. Lipp, *Nature* **1998**, *395*, 645.

[180] J. Wagner, Y. X. Li, J. Pearson, J. Keizer, *Biophys. J.* **1998**, *75*, 2088.

[181] Y. H. Tang, J. L. Stephenson, H. G. Othmer, *Biophys. J.* **1996**, *70*, 246.

[182] I. Bezprozvanny, J. Watras, B. E. Ehrlich, *Nature* **1991**, *351*, 751.

[183] J. B. Parys, S. W. Sernett, S. Delisle, P. M. Snyder, M. J. Welsh, K. P. Campbell, *J. Biol. Chem.* **1992**, *267*, 18776.

[184] A. Atri, J. Amundson, D. Clapham, J. Sneyd, *Biophys. J.* **1993**, *65*, 1727.

[185] H. Kasai, G. J. Augustine, *Nature* **1990**, *348*, 735.

[186] G. Dupont, L. Combettes, L. Leybaert, *Int. Rev. Cytol.* **2007**, *261*, 193.

[187] R. E. Dolmetsch, K. L. Xu, R. S. Lewis, *Nature* **1998**, *392*, 933.

[188] R. S. Lewis, *Biochem. Soc. Trans.* **2003**, *31*, 925.

[189] M. J. Berridge, *Nature* **1997**, *386*, 759.

[190] P. De Koninck, H. Schulman, *Science* **1998**, *279*, 227.

[191] N. I. Markevich, J. B. Hoek, B. N. Kholodenko, *J. Cell Biol.* **2004**, *164*, 353.

[192] O. Slaby, D. Lebiedz, *Biophys. J.* **2009**, *96*, 417.

[193] L. F. Olsen, U. Kummer, A. L. Kindzelskii, H. R. Petty, *Biophys. J.* **2003**, *84*, 69.

[194] A. Hunding, *J. Biol. Phys.* **2004**, *30*, 325.

[195] M. Kirschner, T. Mitchison, *Cell* **1986**, *45*, 329.

[196] T. E. Holy, S. Leibler, *Proc. Natl. Acad. Sci. USA* **1994**, *91*, 5682.

[197] R. Wollman, E. N. Cytrynbaum, J. T. Jones, T. Meyer, J. M. Scholey, A. Mogilner, *Curr. Biol.* **2005**, *15*, 828.

[198] G. C. Rogers, N. M. Rusan, M. Peifer, S. L. Rogers, *Mol. Biol. Cell* **2008**, *19*, 3163.

[199] E. Karsenti, I. Vernos, *Science* **2001**, *294*, 543.

[200] A. Khodjakov, R. W. Cole, B. R. Oakley, C. L. Rieder, *Curr. Biol.* **2000**, *10*, 59.

[201] N. M. Mahoney, G. Goshima, A. D. Douglass, R. D. Vale, *Curr. Biol.* **2006**, *16*, 564.

[202] P. R. Clarke, C. M. Zhang, *Nat. Rev. Mol. Cell Biol.* **2008**, *9*, 464.

[203] M. Caudron, G. Bunt, P. Bastiaens, E. Karsenti, *Science* **2005**, *309*, 1373.

[204] P. Kalab, K. Weis, R. Heald, *Science* **2002**, *295*, 2452.

[205] M. Floer, G. Blobel, *J. Biol. Chem.* **1996**, *271*, 5313.

[206] P. Niethammer, P. Bastiaens, E. Karsenti, *Science* **2004**, *303*, 1862.

[207] P. Kaláb, A. Pralle, E. Y. Isacoff, R. Heald, K. Weis, *Nature* **2006**, *440*, 697.

[208] O. J. Gruss, et al., *Cell* **2001**, *104*, 83.

[209] M. V. Nachury, T. J. Maresca, W. G. Salmon, C. M. Waterman-Storer, R. Heald, K. Weis, *Cell* **2001**, *104*, 95.

[210] C. Wiese, A. Wilde, M. S. Moore, S. A. Adam, A. Merdes, Y. X. Zheng, *Science* **2001**, *291*, 653.

[211] A. Khodjakov, L. Copenagle, M. B. Gordon, D. A. Compton, T. M. Kapoor, *J. Cell Biol.* **2003**, *160*, 671.

[212] H. Maiato, C. L. Rieder, A. Khodjakov, *J. Cell Biol.* **2004**, *167*, 831.

[213] C. L. Rieder, *Chromosoma* **2005**, *114*, 310.

4196 www.angewandte.org

© 2010 Wiley-VCH Verlag GmbH & Co. KGaA, Weinheim

Angew. Chem. Int. Ed. **2010**, *49*, 4170–4198

[214] It has been suggested that diffusion of Ran-GTP is facilitated by the reduction of available space/dimensionality, for example, by the ER (S. Dumont, T. J. Mitchison, *Curr. Biol.* **2009**, *19*, 1086 and J. Ellenberg, E. D. Siggia, J. E. Moreira, C. L. Smith, J. F. Presley, H. J. Worman, J. Lippincott-Schwartz, *J. Cell Biol.* **1997**, *138*, 1193). Formation of the spindle in the absence of Ran-GTP has been found in two recent studies (W. C. Earnshaw, M. Carmena, *J. Cell Biol.* **2003**, *160*, 989 and E. Bucciarelli, M. G. Giansanti, S. Bonaccorsi, M. Gatti, *J. Cell Biol.* **2003**, *160*, 993). Hunding proposed a mechanism based on the cooperative binding of destabilizing proteins on microtubules to explain these curious findings (Ref. [194]). For other models and experimental details, see M. Mogilner, R. Wollman, G. Civelekoglu-Scholey, J. Scholey, *Trends Cell Biol.* **2006**, *16*, 88 and M. Glotzer, *Nat. Rev. Mol. Cell Biol.* **2009**, *10*, 9.

[215] S. F. Gilbert, *Developmental Biology*, 7th ed., Sinauer Associates, Sunderland, **2003**.

[216] F. Grinnell, *J. Cell Biol.* **1994**, *124*, 401.

[217] O. Marin, M. Valdeolmillos, F. Moya, *Trends Neurosci.* **2006**, *29*, 655.

[218] J. T. H. Mandeville, M. A. Lawson, F. R. Maxfield, *J. Leukocyte Biol.* **1997**, *61*, 188.

[219] P. Friedl, K. Wolf, *Nat. Rev. Cancer* **2003**, *3*, 362.

[220] K. Kandere-Grzybowska, C. J. Campbell, G. Mahmud, Y. Komarova, S. Soh, B. A. Grzybowski, *Soft Matter* **2007**, *3*, 672.

[221] S. Burlacu, P. A. Janmey, J. Borejdo, *Am. J. Physiol.* **1992**, *262*, C569.

[222] D. Drenckhahn, T. D. Pollard, *J. Biol. Chem.* **1986**, *261*, 12754.

[223] A. Wegner, *J. Mol. Biol.* **1976**, *108*, 139.

[224] I. Fujiwara, S. Takahashi, H. Tadakuma, T. Funatsu, S. Ishiwata, *Nat. Cell Biol.* **2002**, *4*, 666.

[225] The treadmill mechanism in actin networks differs from treadmilling in individual filaments in several aspects. Within the network, new filaments are formed close to the membrane as branches of preexisting filaments with barbed ends elongated and pointed ends capped at the branching points. As the cell moves on, filaments are turned over by debranching, severing, and depolymerization of the pointed ends. Purified actin filaments undergo the treadmill action very slowly, at a rate of ca. $0.04~\mu m\,min^{-1}$, which cannot account for the fast movement of keratocyte cells at ca. $10~\mu m\,min^{-1}$. The faster filament turnover in cells is attributed to a number of actin-binding regulatory proteins. For further details, see T. D. Pollard, G. G. Borisy, *Cell* **2003**, *112*, 453, Y. L. Wang, *J. Cell Biol.* **1985**, *101*, 597, and T. M. Svitkina, G. G. Borisy, *J. Cell Biol.* **1999**, *145*, 1009.

[226] M. A. Wear, D. A. Schafer, J. A. Cooper, *Curr. Biol.* **2000**, *10*, R891.

[227] S. Schaub, S. Bohnet, V. M. Laurent, J. J. Meister, A. B. Verkhovsky, *Mol. Biol. Cell* **2007**, *18*, 3723.

[228] I. L. Novak, B. M. Slepchenko, A. Mogilner, *Biophys. J.* **2008**, *95*, 1627.

[229] A. Mogilner, L. Edelstein-Keshet, *Biophys. J.* **2002**, *83*, 1237.

[230] D. Didry, M. F. Carlier, D. Pantaloni, *J. Biol. Chem.* **1998**, *273*, 25602.

[231] J. L. McGrath, Y. Tardy, C. F. Dewey, J. J. Meister, J. H. Hartwig, *Biophys. J.* **1998**, *75*, 2070.

[232] By denoting the concentration of actin monomers as c_A, the rate of the first order polymerization reaction is $dc_A/dt = -kc_A$. This solves to give $c_A/c_0 = \exp(-kt)$, where c_0 is the initial concentration and $1/k$ is the characteristic time to achieve the concentration ratio c_A/c_0, which represents the rate of "decay" of monomeric actin.

[233] The results of some experiments suggest that the speed of G-actin delivery to the leading edge exceeds $5~\mu m\,s^{-1}$ (D. Zicha, I. M. Dobbie, M. R. Holt, J. Monypenny, D. Y. H. Soong, C. Gray, G. A. Dunn, *Science* **2003**, *300*, 142), which is difficult to explain by pure diffusion, and has been speculated to involve hydrodynamic flow within the cell. One way to induce such a flow is through pressure differences: lower pressure in the regions where the cell extends protrusions (that is, at the cell front) and higher pressure in the regions where it contracts (at the cell rear). The flow from locations of high to low pressure would then deliver G-actin to the cell front. The validity of this scenario, however, has been questioned and authors such as Novak (Ref. [228]) argue that pressure-driven flows do not have a significant effect on the distribution of G-actin.

[234] J. W. Dai, M. P. Sheetz, X. D. Wan, C. E. Morris, *J. Neurosci.* **1998**, *18*, 6681.

[235] J. W. Dai, M. P. Sheetz, *Biophys. J.* **1999**, *77*, 3363.

[236] D. Raucher, M. P. Sheetz, *J. Cell Biol.* **1999**, *144*, 497.

[237] C. A. Erickson, *J. Cell Sci.* **1980**, *44*, 187.

[238] N. O. Petersen, W. B. McConnaughey, E. L. Elson, *Proc. Natl. Acad. Sci. USA* **1982**, *79*, 5327.

[239] V. C. Abraham, V. Krishnamurthi, D. L. Taylor, F. Lanni, *Biophys. J.* **1999**, *77*, 1721.

[240] E. S. Chhabra, H. N. Higgs, *Nat. Cell Biol.* **2007**, *9*, 1110.

[241] M. Abercrombie, J. E. Heaysman, S. M. Pegrum, *Exp. Cell Res.* **1970**, *60*, 437.

[242] R. Shlomovitz, N. S. Gov, *Phys. Rev. Lett.* **2007**, *98*, 168103.

[243] N. S. Gov, A. Gopinathan, *Biophys. J.* **2006**, *90*, 454.

[244] A. Veksler, N. S. Gov, *Biophys. J.* **2007**, *93*, 3798.

[245] D. Raucher, M. P. Sheetz, *J. Cell Biol.* **2000**, *148*, 127.

[246] A. Mogilner, B. Rubinstein, *Biophys. J.* **2005**, *89*, 782.

[247] A. Hall, *Science* **1998**, *279*, 509.

[248] T. M. Svitkina, E. A. Bulanova, O. Y. Chaga, D. M. Vignjevic, S. Kojima, J. M. Vasiliev, G. G. Borisy, *J. Cell Biol.* **2003**, *160*, 409.

[249] D. Vignjevic, S. Kojima, T. Svitkina, G. G. Borisy, *J. Cell Biol.* **2006**, *174*, 863.

[250] Y. S. Aratyn, T. E. Schaus, E. W. Taylor, G. G. Borisy, *Mol. Biol. Cell* **2007**, *18*, 3928.

[251] S. H. Zigmond, M. Joyce, J. Borleis, G. M. Bokoch, P. N. Devreotes, *J. Cell Biol.* **1997**, *138*, 363.

[252] C. A. Parent, P. N. Devreotes, *Science* **1999**, *284*, 765.

[253] P. A. Iglesias, P. N. Devreotes, *Curr. Opin. Cell Biol.* **2008**, *20*, 35.

[254] C. Janetopoulos, R. A. Firtel, *FEBS Lett.* **2008**, *582*, 2075.

[255] H. Meinhardt, A. Gierer, *Bioessays* **2000**, *22*, 753.

[256] H. Meinhardt, *J. Cell Sci.* **1999**, *112*, 2867.

[257] B. Kutscher, P. Devreotes, P. A. Iglesias, *Sci. STKE* **2004**, pl3.

[258] A. Levchenko, P. A. Iglesias, *Biophys. J.* **2002**, *82*, 50.

[259] R. Skupsky, W. Losert, R. J. Nossal, *Biophys. J.* **2005**, *89*, 2806.

[260] L. Ma, C. Janetopoulos, L. Yang, P. N. Devreotes, P. A. Iglesias, *Biophys. J.* **2004**, *87*, 3764.

[261] H. Levine, D. A. Kessler, W. J. Rappel, *Proc. Natl. Acad. Sci. USA* **2006**, *103*, 9761.

[262] A. Narang, K. K. Subramanian, D. A. Lauffenburger, *Ann. Biomed. Eng.* **2001**, *29*, 677.

[263] K. K. Subramanian, A. Narang, *J. Theor. Biol.* **2004**, *231*, 49.

[264] We make two general comments about the model: 1) The need for a Turing-like mechanism. If A and I were both immobile or were both diffusing at the same rate, the cell would be incapable of sensing chemoattractant gradients. In either of these cases, A and I would be present at similar concentrations throughout the cell, and the effects of activation and inhibition would effectively cancel out, thus leading to a spatially homogeneous distribution of R [see Eq. (22)]. 2) Predictions of the model: I is polarized in the same direction as R because I is activated by S [this is reflected by the second term on the right-hand side of Eq. (21), where the rate of growth of I is proportional to S].

[265] The LEGI model, for example, also accounts for the experimental observation that when the cell experiences a spatially homogeneous increase in the concentration of the

chemoattractant, it "adapts" by transiently increasing the concentrations of both *A* and *I*. These concentrations later drop to the initial, steady-state values.

[266] A. T. Sasaki, C. Chun, K. Takeda, R. A. Firtel, *J. Cell Biol.* **2004**, *167*, 505.

[267] C. Janetopoulos, L. Ma, P. N. Devreotes, P. A. Iglesias, *Proc. Natl. Acad. Sci. USA* **2004**, *101*, 8951.

[268] A. S. Mikhailov, G. Ertl, *ChemPhysChem* **2009**, *10*, 86.

[269] J. Horvath, I. Szalai, P. De Kepper, *Science* **2009**, *324*, 772.

[270] I. R. Epstein, J. A. Pojman, *An Introduction to Nonlinear Chemical Dynamics: Oscillations, Waves, Patterns and Chaos*, Oxford University Press, New York, **1998**.

[271] I. R. Epstein, K. Showalter, *J. Phys. Chem.* **1996**, *100*, 13132.

[272] V. Castets, E. Dulos, J. Boissonade, P. Dekepper, *Phys. Rev. Lett.* **1990**, *64*, 2953.

[273] D. E. Strier, S. P. Dawson, *PLoS ONE* **2007**, *2*, e1053.

[274] K. J. M. Bishop, C. E. Wilmer, S. Soh, B. A. Grzybowski, *Small* **2009**, *5*, 1600.

[275] a) K. Kandere-Grzybowska, C. Campbell, Y. Komarova, B. A. Grzybowski, G. G. Borisy, *Nat. Methods* **2005**, *2*, 739; b) G. Mahmud, C. J. Campbell, K. J. M. Bishop, Y. A. Komarova, O. Chaga, S. Soh, S. Huda, K. Kandere-Grzybowska, B. A. Grzybowski, *Nat. Phys.* **2009**, *5*, 606.

[276] R. Gallagher, T. Appenzeller, *Science* **1999**, *284*, 79.

[277] J. Crank, *The Mathematics of Diffusion*, Oxford University Press, London, **1975**.

[278] R. Matteoni, T. E. Kreis, *J. Cell Biol.* **1987**, *105*, 1253.

[279] E. Nielsen, F. Severin, J. M. Backer, A. A. Hyman, M. Zerial, *Nat. Cell Biol.* **1999**, *1*, 376.

[280] D. R. C. Klopfenstein, F. Kappeler, H. P. Hauri, *EMBO J.* **1998**, *17*, 6168.

[281] I. M. Kulic, A. E. X. Brown, H. Kim, C. Kural, B. Blehm, P. R. Selvin, P. C. Nelson, V. I. Gelfand, *Proc. Natl. Acad. Sci. USA* **2008**, *105*, 10011.

[282] M. Kloc, N. R. Zearfoss, L. D. Etkin, *Cell* **2002**, *108*, 533.

[283] N. Hirokawa, R. Takemura, *Nat. Rev. Neurosci.* **2005**, *6*, 201.

[284] J. S. Tabb, B. J. Molyneaux, D. L. Cohen, S. A. Kuznetsov, G. M. Langford, *J. Cell Sci.* **1998**, *111*, 3221.

[285] S. L. Rogers, V. I. Gelfand, *Curr. Biol.* **1998**, *8*, 161.

[286] I. Semenova, A. Burakov, N. Berardone, I. Zaliapin, B. Slepchenko, T. Svitkina, A. Kashina, V. Rodionov, *Curr. Biol.* **2008**, *18*, 1581.

[287] V. Mermall, P. L. Post, M. S. Mooseker, *Science* **1998**, *279*, 527.

[288] L. Sherwood, *Fundamentals of Physiology: A Human Perspective*, 3rd ed., Brooks/Cole, Belmont, CA, **2005**.

[289] M. Falcke, *Adv. Phys.* **2004**, *53*, 255.

[290] C. A. Athale, A. Dinarina, M. Mora-Coral, C. Pugieux, F. Nedelec, E. Karsenti, *Science* **2008**, *322*, 1243.

[291] T. E. Schaus, E. W. Taylor, G. G. Borisy, *Proc. Natl. Acad. Sci. USA* **2007**, *104*, 7086.

[292] D. Kostrewa, F. K. Winkler, *Biochemistry* **1995**, *34*, 683.

[293] J. V. Small, B. Geiger, I. Kaverina, A. Bershadsky, *Nat. Rev. Mol. Cell Biol.* **2002**, *3*, 957.

[294] J. Ptacek, et al., *Nature* **2005**, *438*, 679.